Review: Current Research on clouds and Precipitation in my Laboratory

T. N. Krishnamurti, Anu Simon, Akhilesh Mishra, Lisa Bucci, Edward Bensman, and A Thomas

Florida State University
Tallahassee, Florida, 32306

Abstract

This talk covers a summary of current research in my laboratory in the areas of precipitation and clouds. There are four parts to this talk; the first part covers the area of breaks in summer monsoon rains over India. Here we show that there are a number of antecedents to the breaks that emanate from North Africa, they relate to positions of the North Atlantic equatorial trough, the local Hadley cell over North Africa, stronger than normal subtropical jet stream over the southern Mediterranean, large amplitude middle latitude wave activity north of the subtropical jet stream, formation of a deep upper tropospheric blocking high over Arabia, conveyance of dry descending air from the northern reaches of this blocking high towards the Arabian sea and as far as central India and the resulting break in the monsoon rains. This scenario lasting for several weeks is confirmed by data sets from the MODIS and CLOUDSAT that portray this extreme dryness and its emanation from the North West of India. The second part of my talk is on cloud flare ups in hurricanes that can often be seen from aircraft flight surveillance and from rapid scan IR imagery at very high resolutions along the inner eye wall of hurricanes. Very high resolution hurricane model forecasts do show such flare ups and can be seen in the fields of liquid or rain water mixing ratios. Model outputs show that such flare ups are followed up with rapid growth of convergence beneath these rapidly growing cloud clusters, a rapid increase of convergence also is intimately related to a rapid increase in the departure from gradient wind balance in these hurricanes, that departure calls for local super gradient winds, we identify that as a rapid intensification of the hurricane. A component of a major field experiment, scheduled for the period August 15 to September 30 2010 (called GRIP, PREDICT, IFEX) will provide dense observations from as many as 7 research aircraft and an unmanned aerial vehicle (UAV) to make measurements needed to portray an observational validation of this scenario. The third and fourth part of my talk deal with multimodel ensemble forecasts for clouds and precipitation. These studies strongly convey the need for post processing of multimodel forecasts, such as the FSU multimodel superensemble, since they invariably carry the highest skills compared to any of the member models.

1. Introduction

This talk covers a few important areas of current research at Florida State University on the topic of clouds and precipitation. This includes studies on cloud transitions from wet to dry spells of the summer monsoon, cloud bursts and rapid intensification of hurricanes, physical initialization for monsoon rains and forecast impacts at mesoscale resolutions and multimodel super-ensemble based cloud forecasts using the TIGGE/ISCCP data sets and precipitation forecast skills at 4km resolution over the US using the WSR88 radar and dense raingauge data sets.

2. Dry air incursions from west Asia and dry spells of the monsoon

A major new finding on the role of the incursion of dry air from west Asia, (Krishnamurti et al., 2010), for the occurrences of dry spells and resulting below normal seasonal rains and droughts over India, is the topic of this section. The following is a short summary of these findings:

2.1. Trajectories

The daily total of rainfall (mm/day) over India for 2009 is shown by a histogram in Figure 1, covering the entire monsoon season. This illustration for the summer of 2009 identifies the dry and wet spells and the long term (40-year) average daily rainfall climatology. In year 2009, except for short wet spells, most of the season carried below normal rains. The distribution of humidity averaged for the dry and wet spells of the Indian monsoon, during the 2009 season, shows a marked drop of humidity at the 700 hPa level for the respective dry and wet spells, Fig. 2 (a-b). The dry spell composite, over several events, clearly shows an extension of a dry tongue extending towards India from the northwest. An almost total absence of clouds was noted in the CLOUDSAT data sets during the break spells of the summer monsoon over India during the 2009 season. Those are illustrated in Fig 2 (d). The CLOUDSAT data displayed in Figure 2 (c) and (d) illustrations carry the satellite passage swaths across India, the raw radiances (level 1data sets), the radar reflectivity, the cloud mask and the cloud types. One of the figures is for active spells, fig. 2 (c), and fig. 2 (d) covers the dry spells of the monsoon. This is a very useful data set since it even goes towards identifying the cloud types, which is a major accomplishment of the CLOUDSAT. The dryness of the wet spells is so large that we see a complete absence of clouds during the breaks. Figure 3(a-c) shows MODIS (MODerate Resolution Imaging Spectroradiometer) imagery composite at the frequency 550nm. This is in the visible part of the spectrum. This shows the incursion of fine dust from the Arabian Sea into all of northern India during periods of composite dry spells. This includes the dry spell composite for the years 2000-2009, (Rajeevan et al., 2006) of the summer monsoon for the following periods. This covers a period between days -3, 0 and +3 of the dry spell composite. The day zero is the day of onset of the dry spell defined following (Rajeevan et al., 2006). The desert regions do not carry a large dust content in the MODIS imagery because the reflected solar radiation over these high albedo regions masks the presence of large dust levels dust even though the dust originates from there. It is quite clear from these composites a large incursion of dust from the west makes its way into northern India during the dry spells.

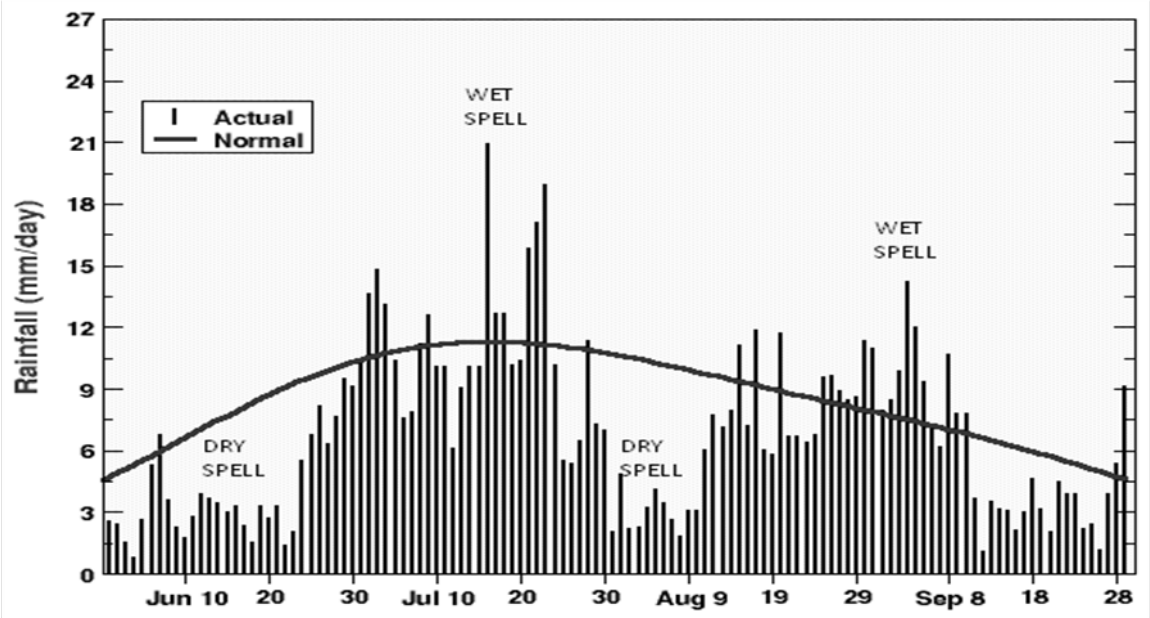

Figure 1: The daily rainfall (mm/day) for the 2009 season over India. The dry and wet spells for the season are identified.

This suggested the need for the construction of a swath of trajectories (Krishnamurti and Bounoua, 1996) that terminate over central India during the dry and wet spells**.** Three-dimensional wind data sets were obtained from the reanalysis fields (Kalnay et al., 1996). Several 10-day long back trajectories terminating over central India were constructed. Parcels of air that terminate over central India at the 850 hPa (roughly 1.5 Km above the earth's surface) level with those that terminate at the 700hPa level (roughly 3 Km above the earth's surface) were distinctly different. During the dry spells, back trajectories, terminating at the 850 hPa level (and above) over central India were of oceanic origin, whereas those arriving at the 700 hPa (and above) level had their origin over west Asia. During the wet spells most of the trajectories, terminating over central India, at 850 and 700 hPa levels were of oceanic origin. Figure 4 (a-h) shows several examples of these back trajectories for a number of wet and dry spells of the Indian summer monsoon covering different years based on the data provided in Rajeevan et al., (2006). The swaths of trajectories from west Asia during the dry spells show a marked descent, as they arrive over central India at the 700hPa level from levels as high as the 400hPa (roughly 6 Km above the earth's surface) level over west Asia. The air in the lowest kilometer is consistently of oceanic origin. Clouds do not show a vertical build up due to the entrainment of very dry air of desert origin above the 3 km level. This is a unique aspect of the dry spells. During the wet spells almost all trajectories, examined, carry more moisture at the 3 km level and a vertical growth of deep convection is not inhibited. Nearly all 10-day long trajectories terminating over central India during dry spells, between 700 and 300 hPa levels, arrive from west Asia, whereas most of the trajectories of the wet spells, terminating over central India are of oceanic origin.

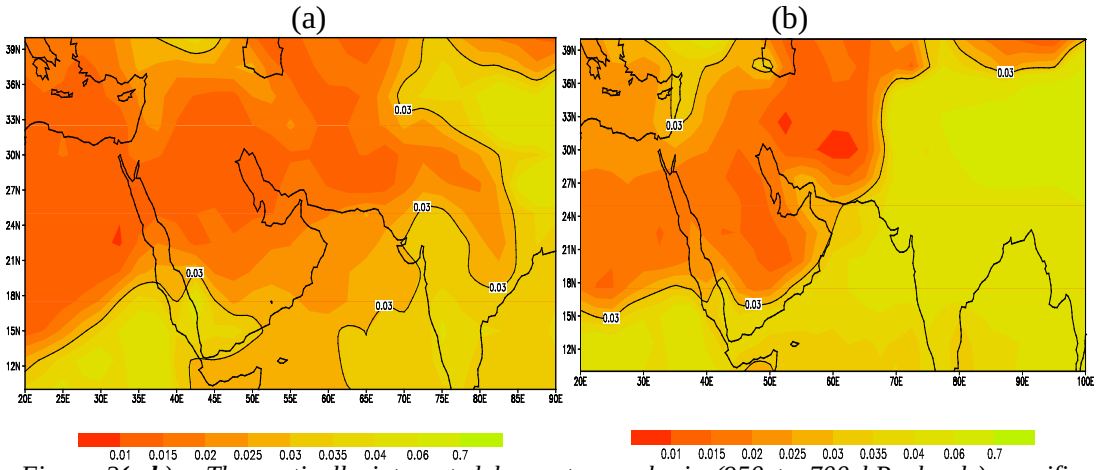

*Figure 2**(a-b)**: The vertically integrated lower tropospheric (950 to 700 hPa levels) specific humidity (kg/kg) for dry and wet spells of monsoon rains over central India. This covers an average for the period (a) June 10 to 19, 2009 for the dry spell and; (b) July 14 to 20, 2009 for a wet spell.*

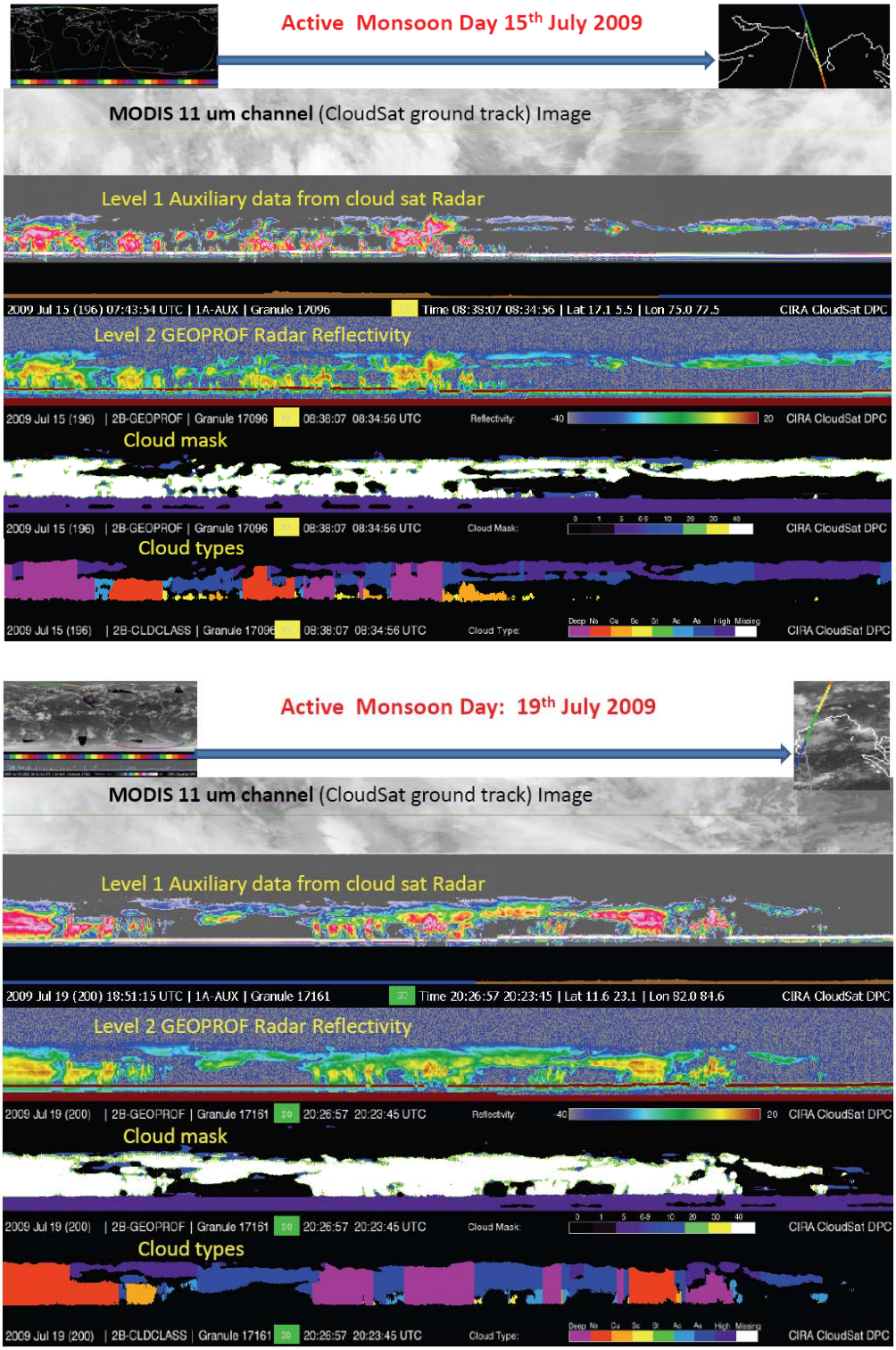

Figure 2 (c): Cloudsat radar reflectivity, cloud mask, cloud types and MODIS cloud imagery during an Active monsoon phase on 15th and 19th July 2009 respectively.

Figure 2 ***(d)****: Cloudsat radar reflectivity, cloud mask, cloud types and MODIS cloud imagery during break monsoon phase on 2nd and 3rd August 2009 respectively.*

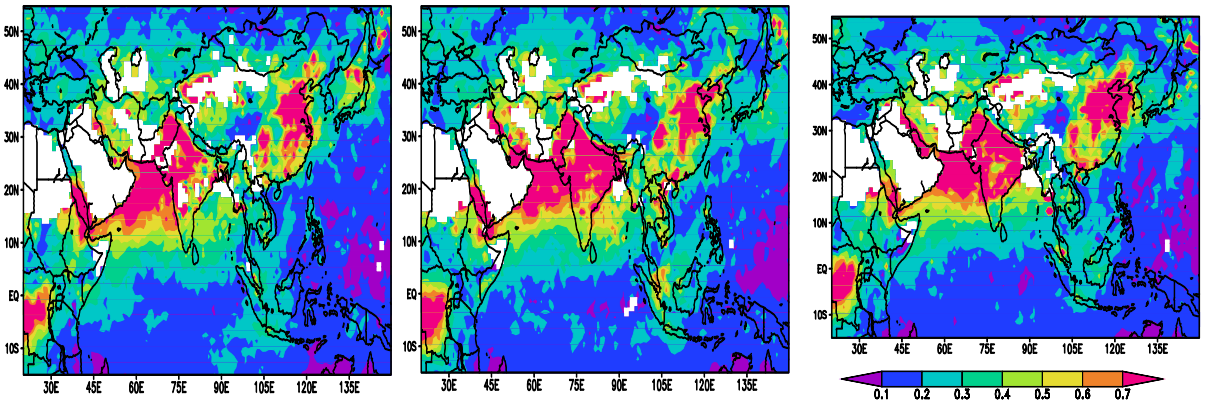

Figure 3 ***(a-c):*** *Aerosol Optical Depth at 550 nm, composited for Break days (2002-2009) from MODIS (Terra/Aqua), (a) 3 days before; (b) 0th day; (c) 3 days after the break. The 550nm wavelength being in visible, MODIS is not able to capture AOD at Deserts.*

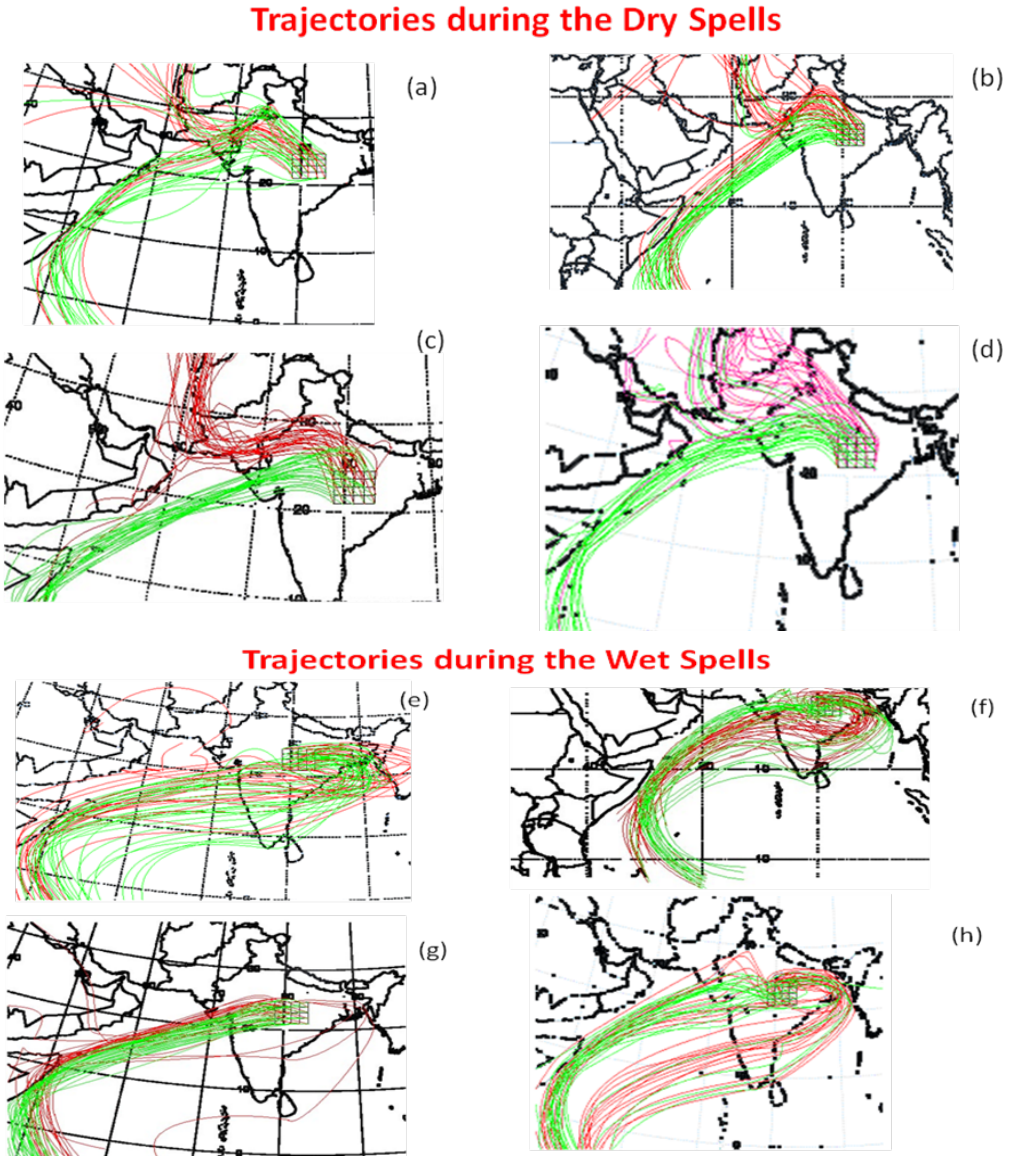

*Figure 4****(a-h):*** *10 day back trajectories from Central India. Left panel illustrations cover dry spell for trajectories terminating at the 850 (green) and 700 (red), the right panel covers the same for trajectories for the wet spells of the Indian summer monsoon. (a) 18 June 2009; (b) 14 August 2005; (c) 16 July 2002; (d) 30 August 2001; (e) 14 July 2009; (f) 01 August 2005; (g) 31 August 2002; (h) 12 July 2001.*

2.2. West Asian Blocking High

The termination points of the 10-day back trajectories from central India, illustrated in the previous section, show an anticyclonic traverse from West Asia. That region is characterized by a Blocking High which appears to be a clear antecedent for these dry spells over India. In Krishnamurti et al. (2009) the center of the Blocking High is generally located near 30 degrees north latitude and 40 degrees east longitude during the dry spells of the summer monsoon of India. A northeastwards shift of this high occurs during the wet spells of the summer monsoon. This is a robust quasi-stationary anticyclone, once formed it is known to persist for periods of the order of a few weeks. The clockwise circulation of this Blocking High is a deep tropospheric phenomenon; it can be seen between the 700 and the 300 hPa levels. For convenience we have illustrated this high using the vertically integrated horizontal winds between the 700 and the 300 hPa levels, Fig. 5(a, b). These are two typical examples of the deep tropospheric circulations of the Blocking High. These circulations, covering all of the dry spells, over India, for the years 2000 through 2009 are provided in Krishnamurti et al (2009).This flow pattern shows the passage of desert dry air of West Asia towards the Arabian sea and Central India. During these episodes the air at and above the 3km level over the Arabian Sea and Central India is very dry .The blocking high appears to be a supplier of very dry air during this spell of the Indian monsoon. This desert air is uniquely different from the oceanic air that traverses over central India, through a deep tropospheric layer, Joshi et al (1985), during the wet spells. The most important aspect of this import of dry air, above the 2 km level over India, is the limitation on cloud growth; clouds as they grow entrain this very dry air, with very low specific humidities. The sub cloud layer of this region is still very moist. Organized mesoconvective systems are not sustained in this environment.

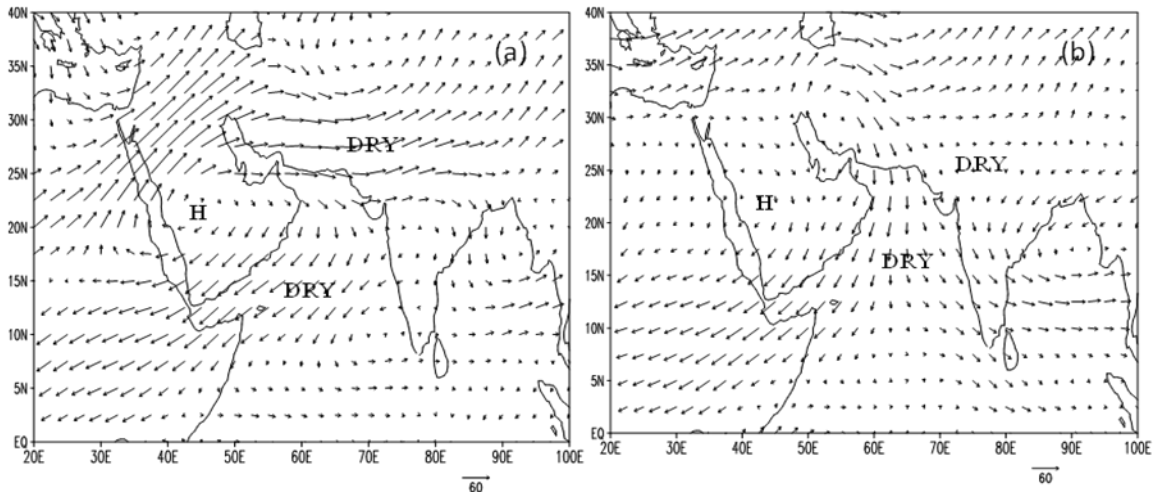

Figure 5 ***(a,b):*** *The blocking high of west Asia for different dry spells of the Indian summer monsoon. These are based on vertically integrated horizontal winds from the 700 to the 300 hPa levels. The lengths of the arrows are defined by the bottom inset in units of* ms^{-1}*. (a) 10 to 19 June 2009; (b) 7 to 14 August 2005;*

2.3. Antecedents of the Blocking High

Using the reanalysis, Kalnay et al (1996), and satellite based IR data sets of several recent decades, during the periods of dry spells over India some of the salient antecedents of the Blocking High over west Asia, Krishnamurti et al (2009) were examined. This section provides a summary of those findings. The ITCZ over the Atlantic Ocean, during the summer months, is located close to 7 N. That line of heavy rainfall climatologically (based on 20 years of data) extends eastwards over North Africa to around 20E longitude. During the dry spells of the Indian summer monsoon that axis of heavy rains is noted to extend poleward by around 2 degrees latitude and eastwards to near 40 E longitudes. The local Hadley Cell over North Africa, computed between the Greenwich Meridian and 50E longitudes, composited over many episodes of dry spells of Indian monsoon, shows a stronger intensity especially between 20 and 25 degrees north latitudes compared to its climatology. At the northern limit of the local Hadley Cell the axis of the subtropical jet stream is located, that was near 27.5 N for these dry spell composites. The subtropical jet stream, over north Africa, has its strongest winds near the 200hPa level with magnitudes around $70ms^{-1}$. Looking at the periods of several of the individual episodes of the dry spells over India, it was noted that winds well in excess of these values are often found. It was furthermore noted that those winds were often stronger than twice the geostrophic value at the 200 hPa level. Those are usually termed as supergradient winds. Supergradient winds are a common feature along the regions of strong subtropical jets, i.e. south of Japan, Krishnamurti et al (2005b); and along the south eastern US, Mogil and Holle (1972). This leg of the subtropical jet stream over the southern Mediterranean also shows such transient features. The atmospheric wind pressure relationship is known to migrate to the anomalous solution of the gradient wind equation with these strong winds lasting for several days. An interesting feature of these strong winds is a strong anticyclonic shear on the equatorward side of the subtropical jet stream. All of these features have been documented in Krishnamurti et al (2009). There is an interesting kinematics of this flow field i.e. the conversion of anticyclonic shear vorticity to anticyclonic curvature vorticity. A formal analysis of this kinematics has been presented by Bell and Keiser (1993) and Viúdez and Haney (1996). It is possible to formally compute this vorticity exchange from shear to curvature in natural coordinates using transformations to latitude/longitude coordinates. That facilitates computations of numerical estimates of this exchange. We have used many cases, related to the dry spell periods of the Indian summer monsoon, and examined the anomalous winds at 200 hPa level, the presence of strong anticyclonic shear and the kinematics of a strong conversion of the shear vorticity to curvature vorticity over North Africa. A strong increase of anticyclonic curvature, from this exchange, relates to the intensification of strongly curved local clockwise flow since the radius of curvature of flow is the inverse of the curvature. That exchange was noted to be large just upstream (westwards) of the region of formation of the Blocking High of west Asia. We noted another feature that contributes to the intensification of the Blocking High over this region. During many periods of the strong dry spells of the Indian summer monsoon, a strong middle latitude wave activity was seen over the latitudes of the Mediterranean. This was portrayed from daily 500 hPa level geopotential height charts. These middle latitude waves, over the longitude belt 30 E to 50E carried a strong tilt from the south west to the north east. That implies a strong northward flux of westerly momentum by these tilted waves. That feature was most pronounced immediately to the north of the subtropical jet stream. A consequence of the removal of westerly momentum from the westerly subtropical jet stream contributes to a weakening of the subtropical jet and a strengthening of eddies of this region. That is a barotropic energetics concept. A formal computation of this tilt related momentum transfer and the energy conversions during many cases of the dry spells of the Indian summer monsoon showed, Krishnamurti et al (2009), that, this process was

robust during the presence of the Blocking High over North Africa. That energy exchange from the zonal flows (the subtropical jet stream) to the eddies of this region (the Blocking High) is an important aspect of the dynamics of this region during the break spells of the Indian summer monsoon. By projecting this scenario for the role of the region to the west of India, and all the way to the Atlantic ITCZ, is viewed as important area for future investigations. Teleconnections are often suggested for phenomenologies that are separated by distances as large as 10,000 km. A lot of dynamics and kinematics transpires within such large distances and the air parcels do face such phenomenology in sequence. Simple relationships between happenings at a point A with respect to responses at a point B (separated by planetary scale distances), are not, generally, that simple to explain. The atmosphere is quite complex in its dynamical and thermodynamical structure over such distances. In summary of this section we note the following elements in a connection of the dry spells of the Indian summer monsoon and the ITCZ over the Atlantic Ocean and North Africa. The ITCZ over the Atlantic and North Africa is north of the climatological position and extends eastwards towards the Red Sea. The local Hadley cell is somewhat stronger during these periods. The subtropical westerly jet stream is stronger and often carries anomalous winds in the context of the gradient wind equation. These features carry a strong anticyclonic shear vorticity. Kinematically the flow fields of this region, near 200 hPa level, favour a strong conversion of the anticyclonic shear vorticity to curvature vorticty. Middle latitude wave motions show a large transfer of energy from the zonal flows to the eddies of this region. That manifests itself as the Blocking High (the prominent eddy of this region). That blocking high extends from 700 to the 300 HPa level over west Asia. Air motions to the north and east of the Blocking High show a strong descent. The transport of this descending air makes the atmosphere above the 2 km level over the Arabian Sea and India very dry during these dry spells of the Indian summer monsoon.

2.4. Modeling

This observational scenario of the dry spells of the Indian Summer monsoon dry spells carries several elements that include the trajectories from west Asia, the Blocking High over west Asia, the strong subtropical jet stream over North Africa with anomalous winds, a strong kinematics of this jet calling for a conversion of shear vorticity into curvature vorticity, tilted middle latitude waves over the southern Mediterranean in the middle troposphere favoring a growth of eddies over this region , and an eastward elongated ITCZ from the Atlantic ocean towards east Africa with a strong local Hadley Cell over this region. It became possible to simulate most of these features from an ensemble modeling using a suite of coupled atmosphere ocean models, Krishnamurti et al., (2000,2005a), Chakraborty et al.(2006), LaRow and Krishnamurti (1998). Those model results clearly show trajectories emanating from West Asian deserts at and above the 700 hPa levels during the dry spell of the year 2009, and arrive over central India. This was a below normal monsoon rainfall year over India.. The model also distinguishes all oceanic trajectories below and above the 700 hPa level during the wet spell of the year 2009, as contrasted from the dry spell that carried oceanic trajectories only below the 800 hPa level. A realistic formation of the Blocking High over west Asia was also clearly simulated from the construction of a multimodel superensemble Krishnamurti et al (1999). The best model of the multimodel suite did form a blocking high over west Asia , but the circulations over the southern Indian ocean carried too strong an easterly wind bias in the lower troposphere, those were corrected and much improved by the multi model superensemble. The multimodel superensemble was also able to predict most of the elements related to these dry spells of the Indian summer monsoon for the 2009 season very well. In particular we noted a clear extension of the Atlantic ocean ITCZ all across Africa near 8N. This modeling and the observational aspects supports the notion of the role of

the dry desert air towards inhibiting the growth of deep convection over India during these dry spells. Illustrations and further details can be found in Krishnamurti et al., (2010).

3. Cloud flare-ups and rapid intensification of hurricanes

This is a cloud related topic of much interest to the hurricane/Typhoon/Tropical Cyclone community. Those that fly hurricane reconnaissance flights often report (e.g. US Air Force C 130 flier Richard Henning) that a cloud flare up along the inner eye wall of a hurricane is often followed up by a rapid intensification of the hurricane. This is a very interesting scientific topic that deserves further research. Hurricane Katrina of 2005 provided some great examples of such flare ups as the hurricane rapidly intensified to a category 5 storm over the Gulf of Mexico. Fig 6 a and b show examples of precipitation and cloud flare ups as seen from TRMM data sets during this phase of Katrina on August 28. Along the eye wall of hurricane Katrina, one can see large, rain events, fig.1a with intensities of the order of 250 mm/day and the vertical built up of cloud flare ups and hydrometeors, as seen from the TRMM radar fig 6 b. This particular feature can also be followed on the rapid scan imagery of the GOES IR film loop (to be presented in the lecture) showing a small life cycle of the order of a few hours.

The GOES imagery shows several such cloud flare ups along the eye wall, although no other data sets (such as winds and temperature profiles) on the scales of these clouds or cloud ensembles such as winds, temperature, moisture and pressure are currently available. A relationship of the cloud flare ups and intensification of winds in hurricanes can be easily seen from the context of departures from balance laws:

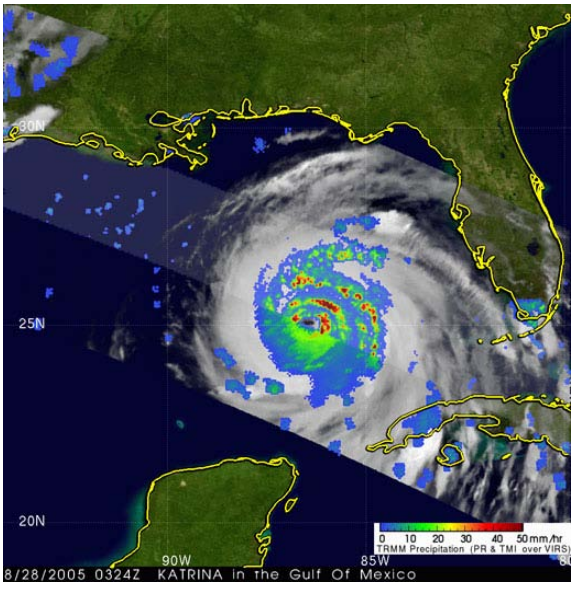

Figure 6 (a): Precipitation and cloud flare ups as seen from TRMM data sets during this phase of Katrina on August 28.

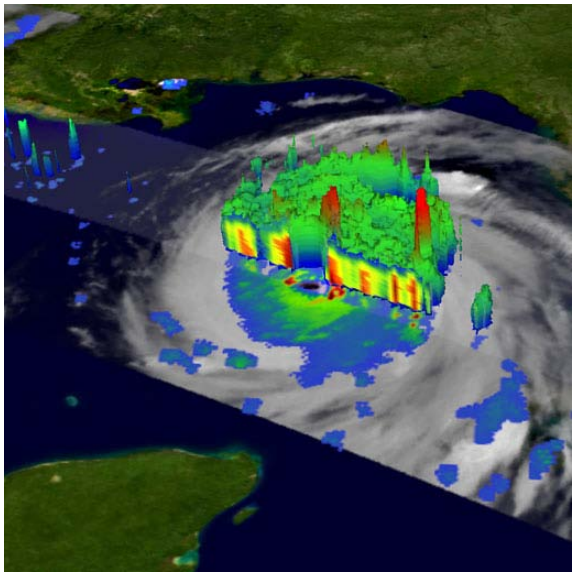

Figure 6 (b): Precipitation and cloud flare ups as seen from TRMM data sets during this phase of Katrina on August 28.

The complete non linear balance equation can be written in the form:

$$-\nabla^2\phi = -f\left(\frac{\partial V_\theta}{\partial y} - \frac{\partial V_r}{\partial x}\right) - 2\left(\frac{\partial V_r}{\partial x}\frac{\partial V_\theta}{\partial y} - \frac{\partial V_\theta}{\partial x}\frac{\partial V_r}{\partial y}\right) + \beta u + \left(\frac{\partial \omega}{\partial x}\frac{\partial V_\theta}{\partial p} + \frac{\partial \omega}{\partial y}\frac{\partial V_r}{\partial p}\right) + D^2 +$$

$$\left(\frac{\partial D}{\partial t} + V_\theta\frac{\partial D}{\partial x} + V_r\frac{\partial D}{\partial y} + \omega\frac{\partial D}{\partial p}\right) + \left(\frac{\partial F_{V_\theta}}{\partial x} + \frac{\partial F_{V_r}}{\partial y}\right) \qquad (1)$$

where the symbols are: D is the horizontal two-dimensional velocity divergence; V_θ and V_r and ω are the components of the total wind V; f is the Coriolis parameter; β is the meridional variation of f; Φ is the geopotential height; and F is the frictional contribution.

The terms defining the so called non linear balance law, Phillips (1966), are

$$\nabla^2\phi = f\nabla^2\psi + 2J\left(\frac{\partial\psi}{\partial x}, \frac{\partial\psi}{\partial y}\right).$$

Note that, those terms that are not within this balance, include the local change of divergence, the horizontal advection of divergence, the vertical advection of divergence , a divergence square term and a quadratic term carrying gradients of vertical velocity. We shall show that model output from very high resolution hurricane forecasts, during cloud flare ups, show a substantial growth of divergence (i.e. growth of low level convergence) and also the growth of departures from balance laws within a model hurricane. Those regions are tagged where the model based rain water mixing ratios shows cloud flare ups. There is a close relationship between the non linear balance law and the gradient wind balance laws. The latter, in a storm centered local cylindrical coordinate, calls for a balance among the coriolis, pressure gradient and the centrifugal force. If one examines the rotational part of the gradient wind balance it is identical to the radial casting of the non linear balance system. The complete radial equation, in local cylindrical coordinates includes the contributions from divergence.

We shall next write down the complete radial equation in storm centered (not storm relative) coordinates

$$\frac{\partial V_r}{\partial t} + V_\theta\frac{\partial V_r}{r\partial\theta} + V_r\frac{\partial V_r}{\partial r} + \omega\frac{\partial V_r}{\partial p} - \frac{V_\theta^2}{r} - fV_\theta = -g\frac{\partial z}{\partial r} + F_r$$

where V_r, V_θ are the radial and azimuthal wind components.

If GWD denotes the terms that describe gradient wind departures, we can write them as:

$$GWD = -\frac{\partial V_r}{\partial t} - V_\theta\frac{\partial V_r}{r\partial\theta} - V_r\frac{\partial V_r}{\partial r} - \omega\frac{\partial V_r}{\partial p} + F_r$$

The complete gradient wind equation is now expressed as:

$$\frac{V_\theta^2}{r} + fV_\theta - g\frac{\partial z}{\partial r} + GWD = 0$$

This quadratic equation has a solution of the form:

$$V_\theta = \frac{-f \pm \sqrt{f^2 - \frac{4}{r}\left(GWD - g\frac{\partial z}{\partial r}\right)}}{\frac{2}{r}}$$

The negative root is non physical since it describes anticyclonic motions, in the lower troposphere. If GWD is strongly negative, i.e. the gradient wind departures are strongly negative then the solution describes supergradient winds. This theoretical scenario of cloud flare ups, rapid growth of lower tropospheric convergence, growth of gradient wind departures and the generation of supergradient winds have been seen in high resolution hurricane model outputs. We shall next illustrate this scenario from a high resolution model output derived from a study of Davis et al (2008). This was a WRF model that was run at a horizontal resolution of 1.33 km. It was triply nested and carried a high resolution, movable, inner nest. It is a nonhydrostatic microphysical model with explicit clouds in the inner nest. This model provided a reasonable track, intensity and landfall for Hurricane Katrina of the 2005 season. Barring some temporal phase errors on the timing of intensity reaching category 5 storms it carried many realistic features in its 36 hour forecast. It became possible to examine this detailed output at intervals of every half hour. The clouds were seen from the output fields of liquid water and the rain water mixing ratios. It was also possible to construct the radar reflectivity as implied by the model hydrometeors. Those bore a close resemblance to the reconnaissance aircraft based observed radar reflectivities. Those details can be seen in Davis et al (2008). Fig 7 shows model based rain water mixing ratios that resemble hurricane structures. A closer examination of these model fields showed frequent cloud flare ups along the inner eye wall of the hurricane. These are short lived clouds whose life cycle covers a few hours. Fig 8 shows one such life cycle of a cloud burst that preceded the rapid intensification of hurricane Katrina in the model output. These are the cloud water mixing ratios showing the rapid growth and decay of one cloud element. This occurred between 15z hours and 18z hours on August 28 2005. The entire scenario of cloud flare ups to the rapid intensification was noted on many instances in the model output. Examples of these are shown in Fig (9-12 a,b,c,d). Here we see a rapid growth of the liquid water mixing ratio along the inner eye wall, implying cloud bursts, of the model hurricane that is followed up with a rapid growth of convergence below the cloud, we see a rapid growth of gradient wind departures and a rapid intensification from the generation of supergradient winds. Those winds come from the solution of the complete radial equation and are also the same as the model predicted winds at those locations. These are very interesting features during the model's intensification of Katrina to a category 5 state. We lack cloud ensemble scale observations at the present time to validate such details. In that context it is worthwhile stating that a forthcoming NASA field experiment, GRIP (Genesis and Rapid Intensification Processes), is designed to provide observations for hurricane intensity studies, this is schematically shown in fig. 13. During the summer of 2010 there will be two aircraft deploying WIND LIDAR inside hurricanes. One is a NOAA P3 and the other is a NOAA WB57. In addition to that almost 9 aircraft will provide dropwindsonde and flight level winds (2 NOAA P3, NOAA G4, NSF G5, DC8, NASA DC8, NASA ER2, AF C130 and a pilot less drone Global Hawk) . Besides that we can expect Rapid Scan winds i.e. cloud tracked winds from GOES geostationary satellites. The period would be August 15 to September 30 of 2010. This data pool, schematically illustrated in fig. 8, is expected to provide several thousand wind observations for the inner core of hurricanes. This schematic illustrates the deployment of research aircraft and the Global Hawk for hurricane surveillances. Two of the aircraft would carry Wind Lidar that utilizes aerosol back scattering for estimating from Doppler shifted winds of the moving targets to estimate horizontal winds. This along with a plethora of dropwindsondes are expected to provide as many as

several thousand wind vectors in three dimensions in the inner core of a hurricane. Several of these aircraft including the Global Hawk will carry radar to monitor the radar reflectivity. Thus we expect to carry out an observational validation of the aforementioned scenario of cloud bursts leading to rapid intensification.

From a current modeling context of hurricane prediction, the following comments may be of interest. As the European Center improves its model and the resolution we have seen the most impressive hurricane track forecasts from their very high resolution model. They also reflect that the intensity forecasts do not carry the same improved skills. Hurricane intensity is a difficult modeling issue since both outer thrusts (outer angular momentum) and inner thrust (clouds and cloud microphysical processes) influence the local intensities. Mesoconvective cloud elements abound along the inner core and we may have to assimilate such elements from vast observations as may become available from the GRIP, PREDICT, IFEX observing systems?

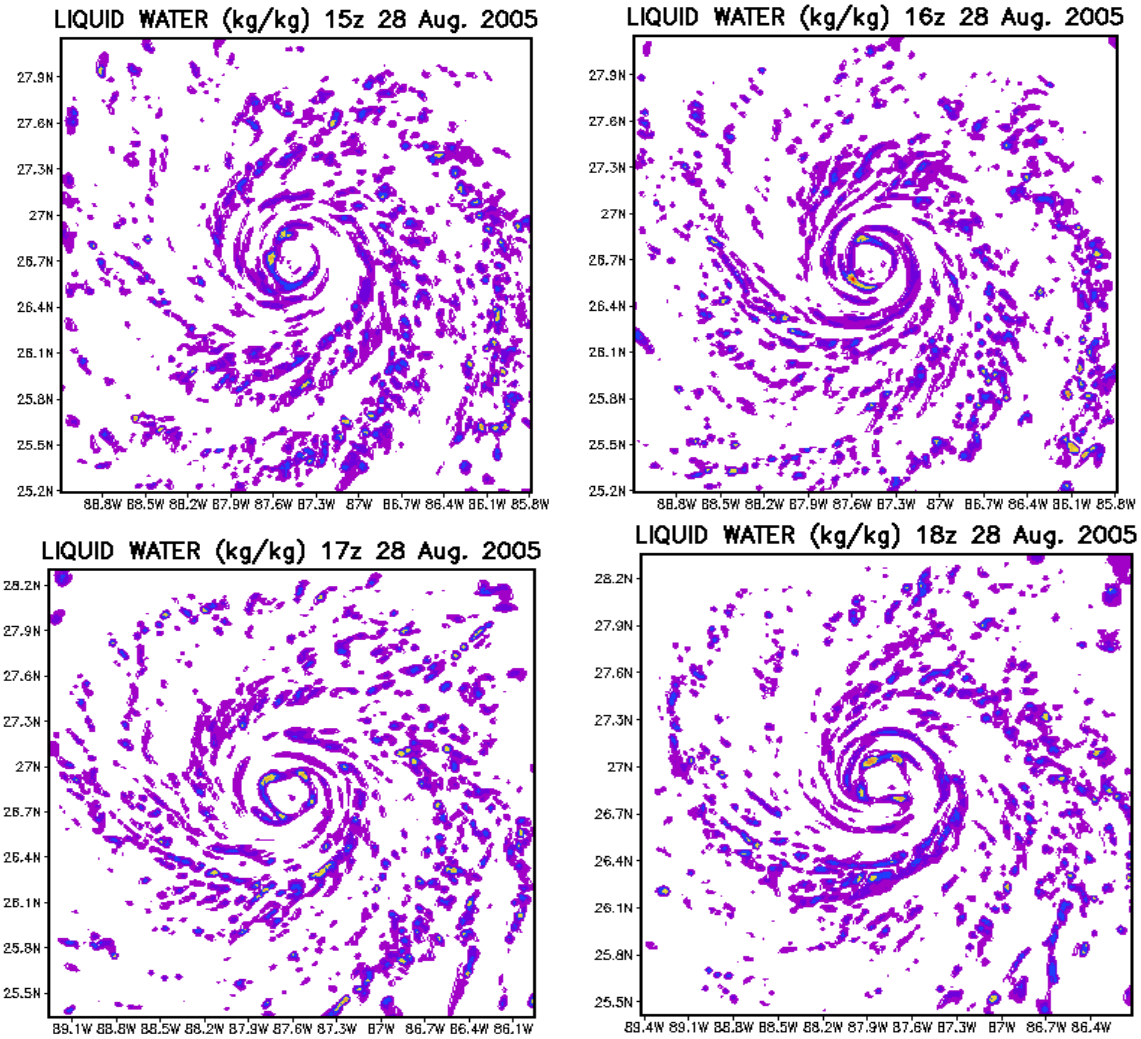

Figure 7: The hourly time history of vertically integrated liquid water from surface to 450hPa levels.

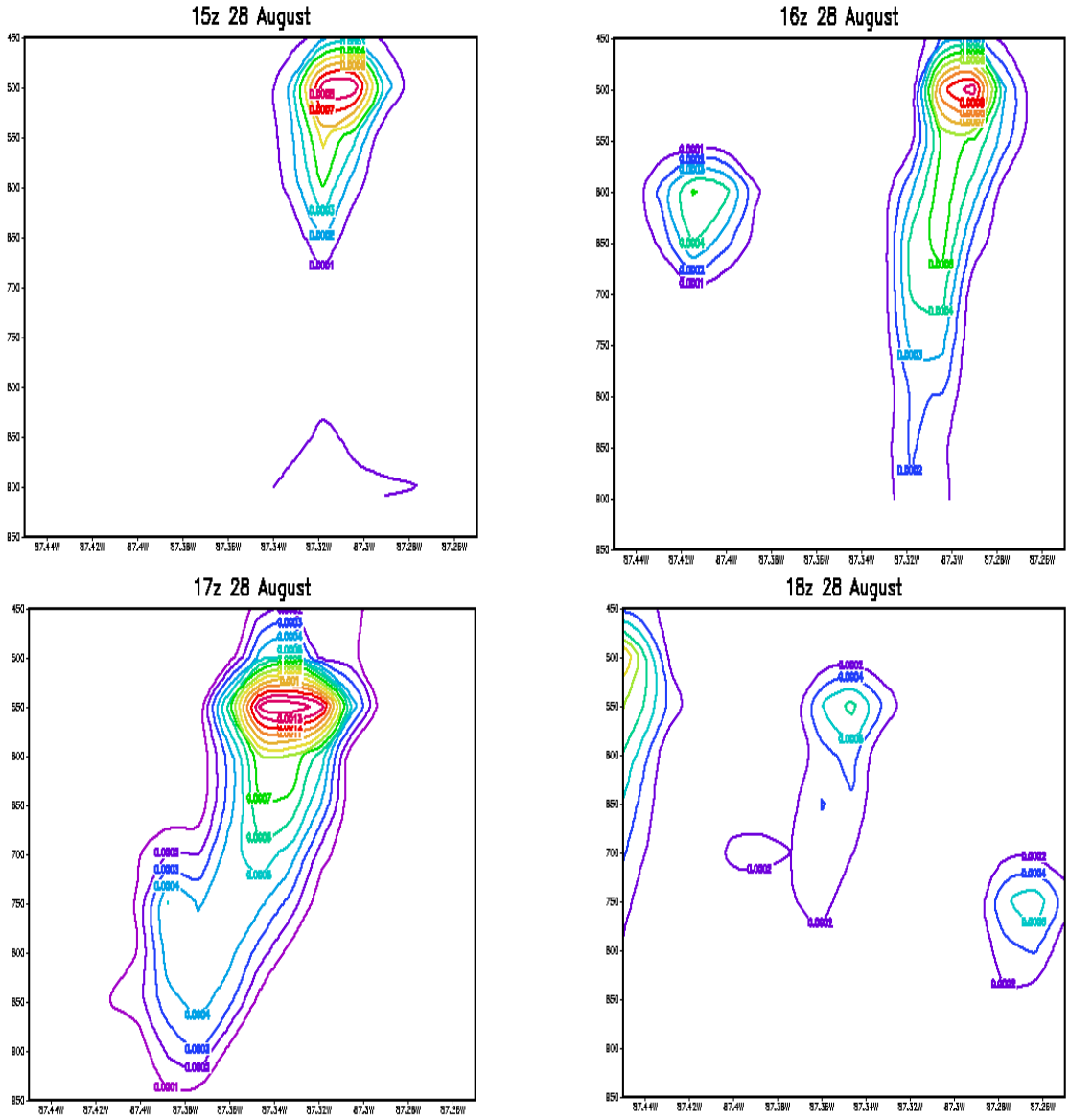

Figure 8: The life cycle of a deep convective cloud

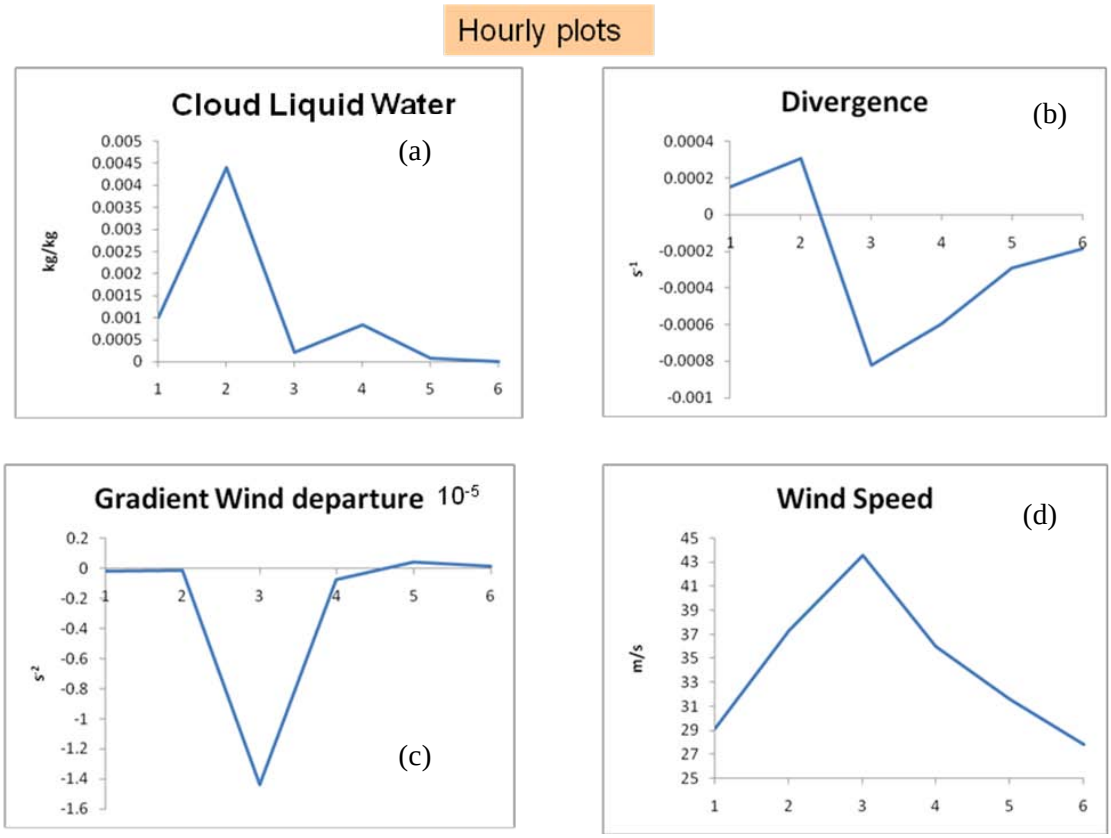

Figure 9: An example of hourly (along abscissa) changes, of the (a) cloud liquid water (kg/kg), (b) divergence s^{-1}, (c) gradient wind departures (x 10^{-5}) and the (d) wind speed (ms^{-1}) , along the ordinates, for the simulated hurricane Katrina on Aug 28 2005 at 14UTC. These are results for a cloud flare up along the inner eye wall.

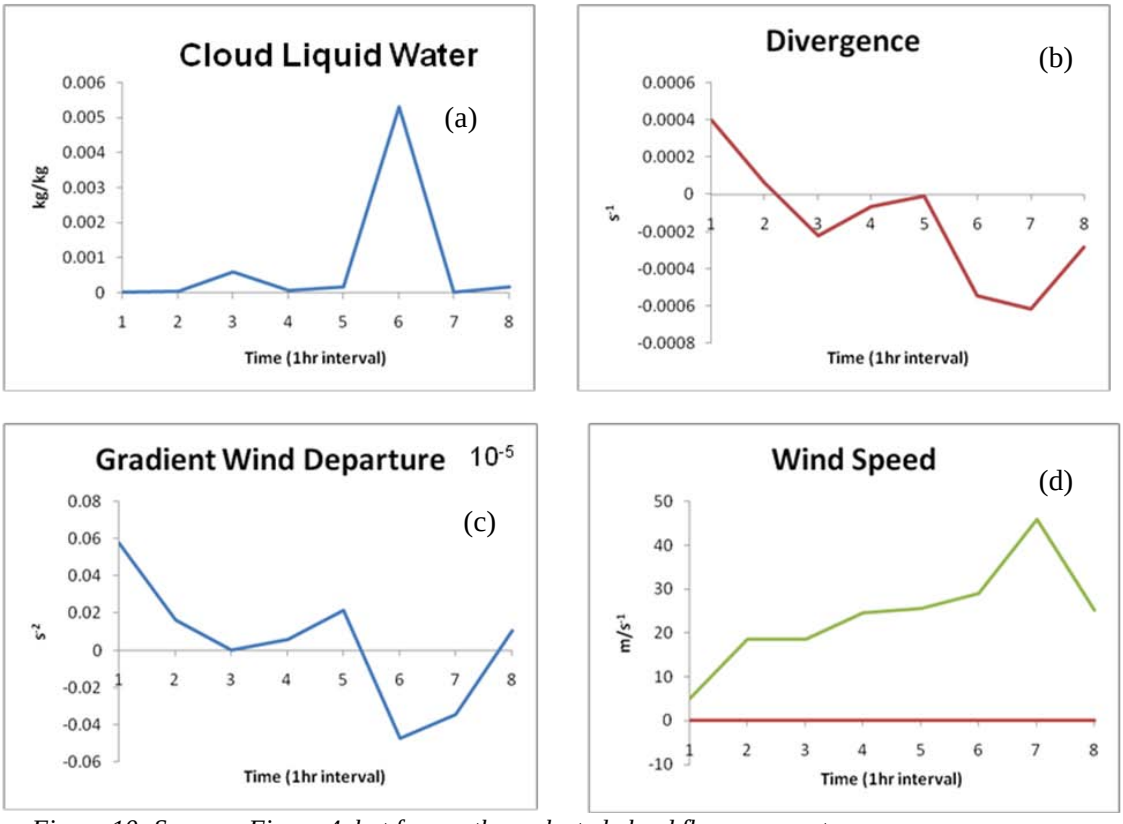

Figure 10: Same as Figure 4 but for another selected cloud flare up event.

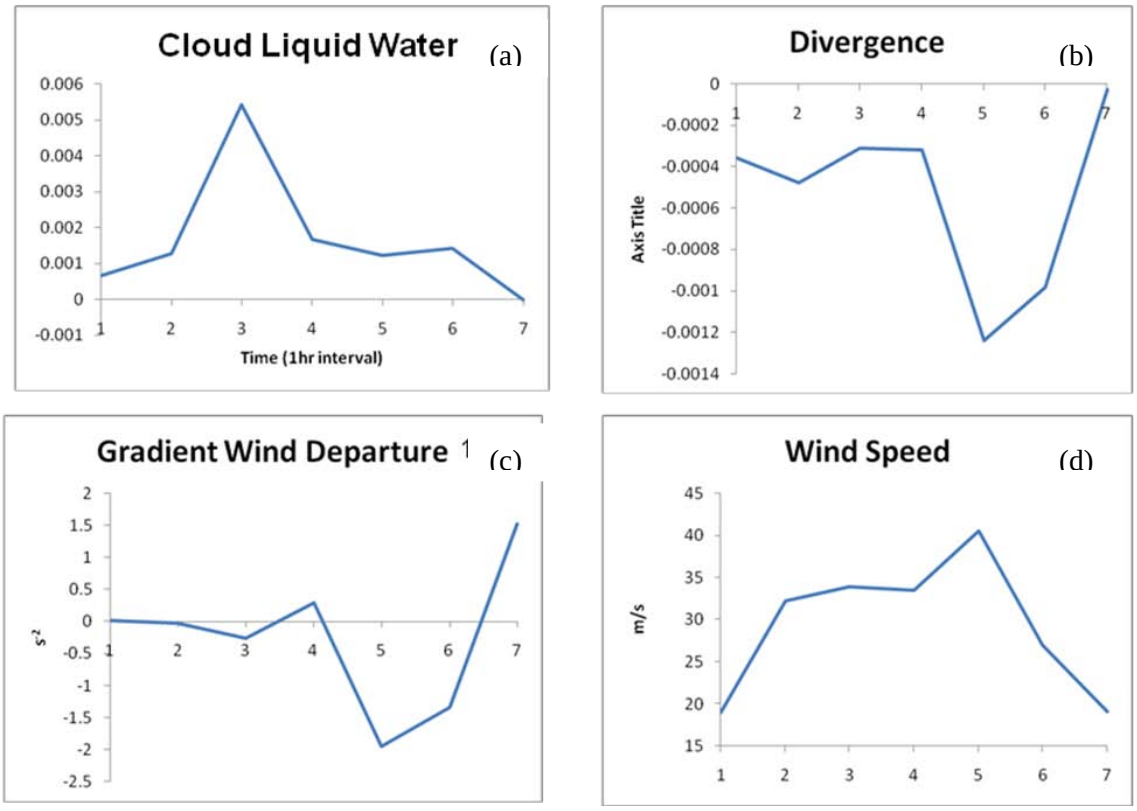

Figure 11: Same as Figure 4 but for another selected cloud flare up event.

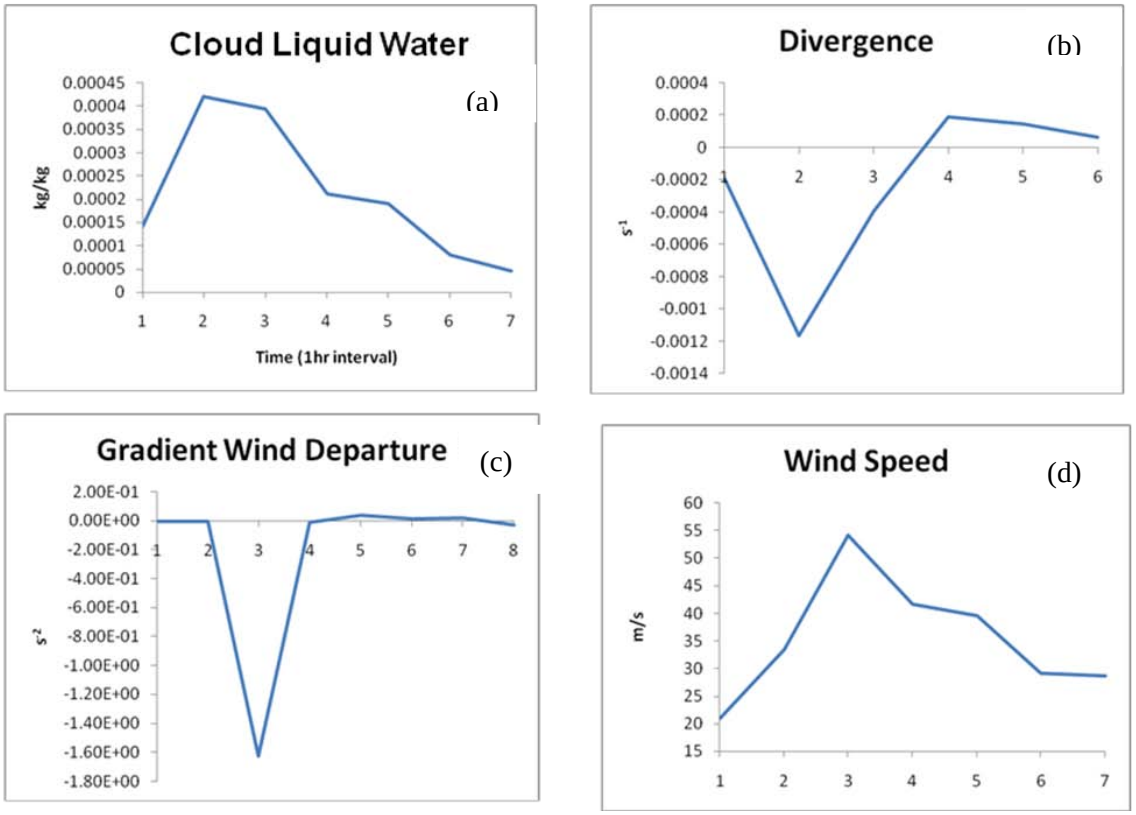

Figure 12: Same as Figure 4 but for another selected cloud flare up event.

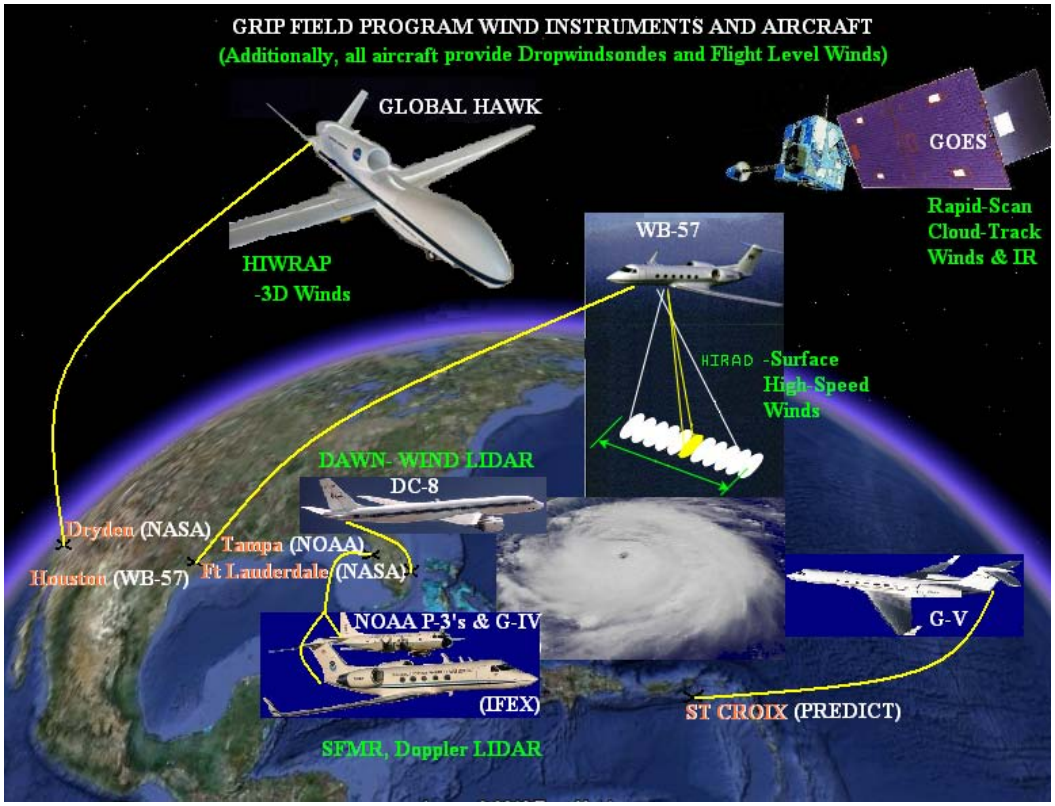

Figure 13: Schematic of the proposed NASA field campaign.

An observational validation of the above scenario of cloud bursts to the rapid intensification is a goal of the field experiment. We also wish ask if one can predict such a scenario. That may take a model at a horizontal resolution of around 500 meters and the clouds and cloud bursts have to be predicted explicitly. Assimilation of the above several thousand wind observations might be needed for a mesoscale model. Predicting the three-dimensional life cycle of clouds may be possible for a first generation of clouds that live for a few hours after the initial time of forecast, the question remains whether a second generation of clouds that form some 5 to 6 hours after the initial state of such a model can be predicted in the right place and time and if such a second generation clouds are to exhibit a flare-up can those be predicted? The prediction of the placement of rapid intensification is of paramount importance for hurricane damage. It is not clear that large scale forcing that is so well predicted by the best models, such as that of ECMWF, can indeed, force the new generation of clouds to form at the correct space-time locations some 12 hours or later after a forecast start time, these are some of the future challenges.

4. Prediction of large scale clouds

It is customary for global modelers to use diagnostic or prognostic clouds and issue forecasts for cloud fractions (within grid squares) for total, low, medium and high clouds. The diagnostic cloud method generally defines clouds as a function of the prevailing relative humidity as compared to certain threshold relative humidities within these cloud layers. Based on satellite based OLR and co located atmospheric soundings of temperature and humidity it is possible to define threshold relative humidities that are found in such clearly defined cloud layers. Prevailing relative humidity's that exceed such thresholds define the occurrence of cloud fractions in such layers. The prognostic cloud method generally adds two more dependent variables in the global model; these are cloud fractions and the cloud water mixing ratio. In addition mechanisms for the growth and decay of clouds are

clearly defined for the cloud liquid water equations. These are now classical methods and details can be found in Gelyn (1981), Slingo (1980, 1987), Sundqvist (1979) and Tiedtke (1993).

This study will address possible improvements in the skills of cloud forecasts, on the medium range, from deploying a suit of global models. FSU has been working its multimodel superensemble methodology, Krishnamurti et al (1999, 2000a, 2000b) for reducing the collective bias errors of the member models as we construct the superensemble forecast. This method works very well if the member models make consistent bias errors in their phase and amplitudes as compared to the observed (analysis) state. This was true for the cloud forecast data sets we derived from the TIGGE files.

4.1. ISCCP Data Sets

These are the International Satellite Cloud Climatology Project data sets. This currently includes data sets from six geostationary and two polar orbiting satellites. These data sets are re-gridded to a 30 km spatial resolution and carry a 3 hourly temporal resolution. Pixel flags in these data sets identify presence of clouds. This data set also includes the cloud top pressure that is used for estimating cloud altitudes.

4.2. TIGGE data sets

These are operational forecast data sets that are provided by the lead global modeling groups of the world to archives at ECMWF, Japan, China and NCAR. Table 1 identifies some of the current models that participate in this data exchange activity. TIGGE archives were initiated in October 2006. The spatial resolution of the participating models vary somewhat, generally they are of the order of 100 km. Total cloud cover predicted by the models is one of the fields that is archived. Most forecasts are of ten days length.

4.3. Methodology for cloud forecasts

A common denominator resolution of one degree latitude/ longitude is used for the tabulation of all total cloud forecast data sets, of all the participating models, towards the construction of the ensemble mean and the superensemble forecasts. A temporal resolution of 24 hours (one forecast per day out to

Table 1. TIGGE Models

Center	Ensemble Members	Model Resolution	Forecast Length
ECMWF	51	N200 (Reduced Gaussian)	10 day
ECMWF	51	N128 (Reduced Gaussian)	10-15 day
UKMO	24	1.25 x 0.83 Deg	15 day
JMA	51	1.25 x 1.25 Deg	9 day
NCEP	21	1.00 x 1.00 Deg	16 day
CMA	15	0.56 x 0.56 Deg	10 day
CMC	21	1.00 x 1.00 Deg	16 day
BOM	33	1.50 x 1.50 Deg	10 day
MF	11	1.50 x 1.50 Deg	2.5 day
KMA	17	1.00 x 1.00 Deg	10 day
CPTEC	15	1.00 x 1.00 Deg	15 day

ten days) is used in this study. We use four major models, ECMWF, GFS, JMA and UK Met. The results shown here pertain to four regions: Global, a monsoon domain (55E to 120E and 30S to 30N), a European domain (30W to 80E and 30N to 70N) and a North America domain (220E to 320E and 15N to 55N). For layer clouds, low, middle and high we did not have the data available for one of the models, for those we reconstructed the low, middle and high clouds using an FSU diagnostic cloud algorithm, Krishnamurti et al 2008. This required a normalization of the cloud fractions using the total cloud cover fraction that was available for that model; we also used the temperature and moisture forecasts of that model in order to test against threshold relative humidities to assign the presence of clouds. In that sense the layer clouds for that model is not representative of that model. The training phase of the superensemble carried 75 days, between October 2006 and January 2007. The forecast phase included 25 days during the month of February 2007. Superensemble weights varied in space and time, those were calculated separately for each day of forecast, this is necessary since the model forecast performance varies as a function of forecast length.

4.4. Prediction of total clouds

The RMS errors of total cloud fractions are computed for the Global, Monsoon domain, North America and Europe. These are the averaged errors for the first 25 days of forecasts for February 2007. The results for days 1, 3 and 5 of forecasts for the JMA, UK Met, ECMWF and the Superensemble are shown in Figure 14 through 17. It is clear that from the construction of the superensemble we can reduce the collective bias errors of the member models and obtain much higher skills for total cloud forecasts. These were consistent improvements at all days of forecasts. These models carried persistently similar errors, thus the superensemble was able to exploit and reduce such errors. Figs 14 (a) shows the spatial correlations of observed and predicted clouds and are shown in the same format as the previous illustration. Figure 14 (b) depicts the RMS errors. Here we see that the construction of the superensemble provides the best total cloud forecasts for days 1, 3 and 5 of forecasts compared to the four member models. In general these results are quite similar for all four domains. The same behavior in the results is seen for the high and middle clouds, shown in figures 15 (a) and 15 (b). Here the forecasts skills for the RMS errors and the spatial correlations, through day 7 of forecasts are displayed for 25 forecasts during February 2007. The superensemble clearly a marked improvement for the layer cloud forecasts. The low cloud forecasts, not shown, were quite similar as well.

4.5. The Great Success of the European Center

Figure 16 shows a comparison of IR based cloud and those from a recent (October 8 2008) version of the ECMWF global model which was run at a horizontal resolution of T1279, (approximately 15km horizontal resolution) these are shown on the right panel. The observed IR imagery from the METOSAT is shown on the left panel. The amount of detail on the cloud structures, that are seen here, are simply phenomenal. This is a great achievement for the ECMWF's model and its data assimilation. This frame is part of a 36 hour animation (will be shown at my presentation), that is available from ECMWF. This animation shows passage of African wave based cloud systems, subtropical stratocumulus and extratropical frontal clouds. At a 15 km resolution, we begin to see such fine details. These were based on their current version of global model.

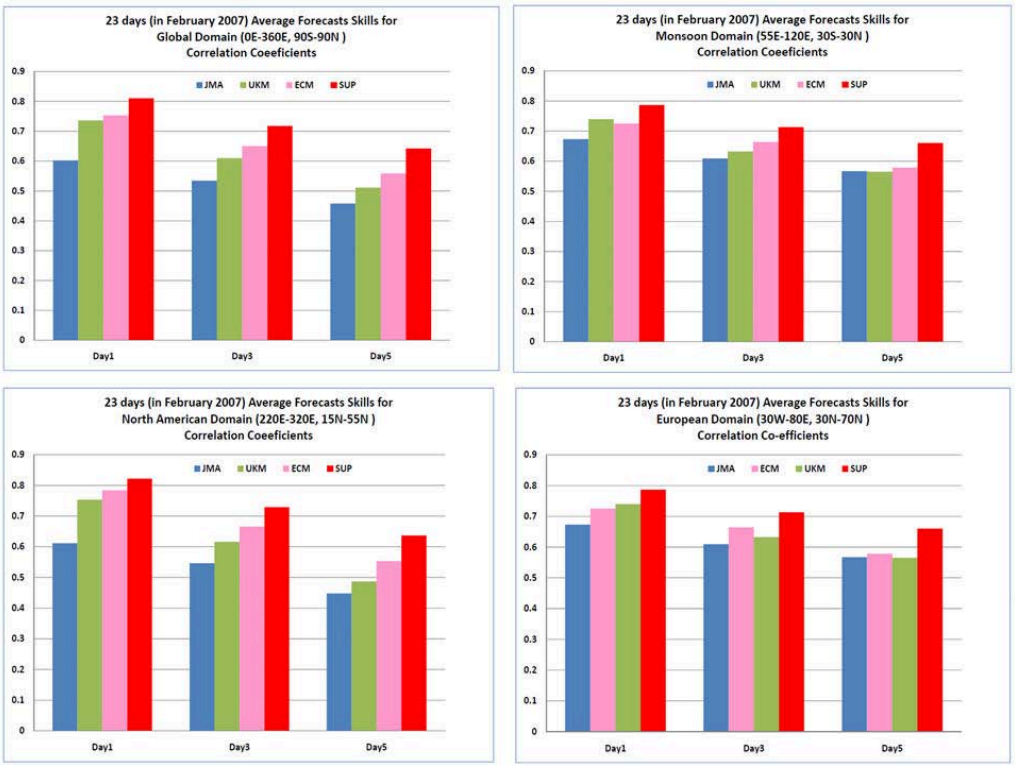

Figure 14 ***(a)****: The spatial correlations of Total Cloud Cover based on 23 days of forecasts, for days 1, 3 and 5 of forecasts. The four panel of diagrams show results for Global domain, Monsoon Domain, North American Domain and European Domain. The four vertical bars from left to right carry the spatial correlations for the models JMA, UK Met, ECMWF and the Multimodel Superensemble.*

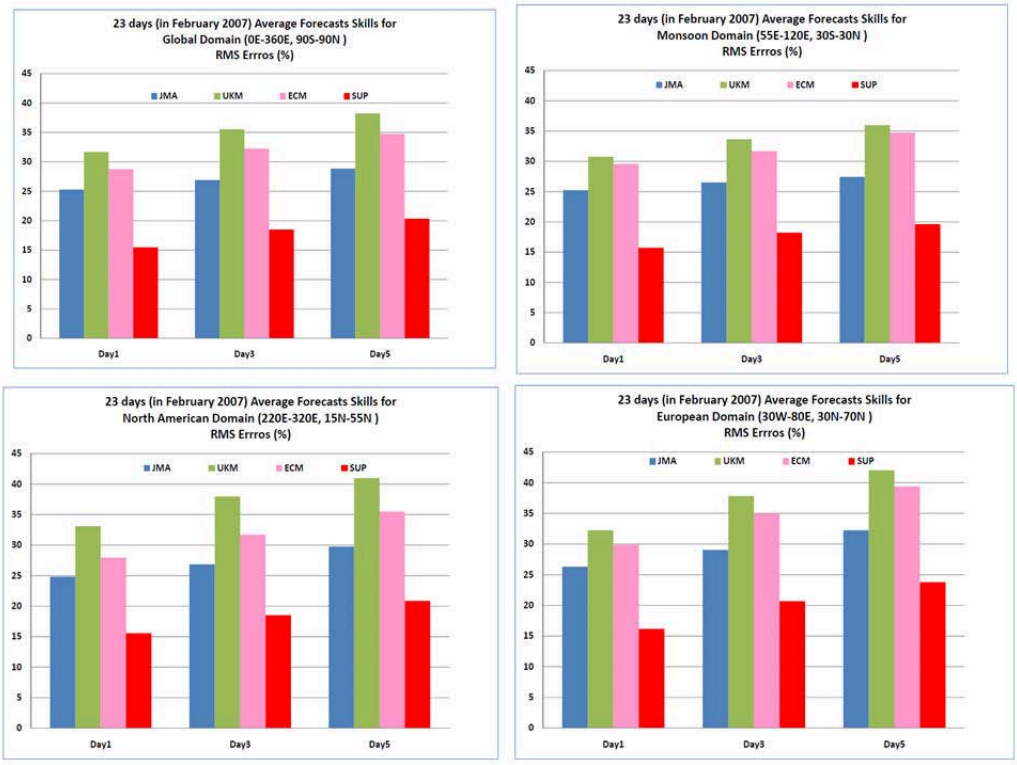

Figure 14 (b)*: The RMS errors of Total Cloud Cover based on 23 days of forecasts, for days 1, 3 and 5 of forecasts. The four panel of diagrams show results for whole Global, Monsoon Domain, North American Domain and European Domain. The four vertical bars from left to right carry the RMS errors for the models JMA, UK Met, ECMWF and the Multimodel Superensemble.*

Results- High Clouds

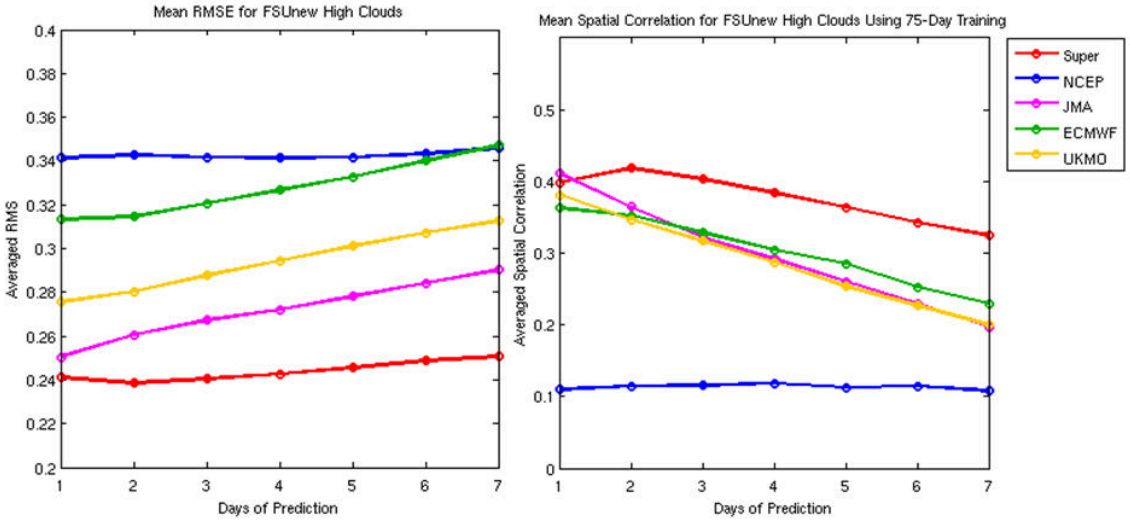

Figure 15 (a): The RMS errors (left) and the spatial correlations (right) through day 7 of forecasts of high clouds, over the global tropics, for the models NCEP/GFS, UK Met, JMA, ECMWF and the Multimodel Superensemble.

Results- Middle Clouds

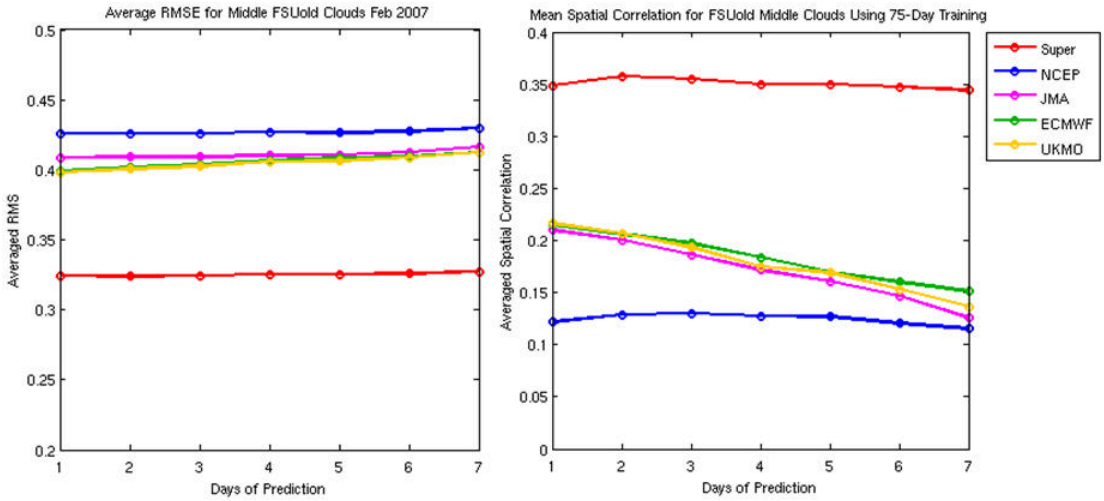

Figure 15 (b): *The RMS errors (left) and the spatial correlations (right) through day 7 of forecasts of middle clouds, over the global tropics, for the models NCEP/GFS, UK Met, JMA, ECMWF and the Multimodel Superensemble.*

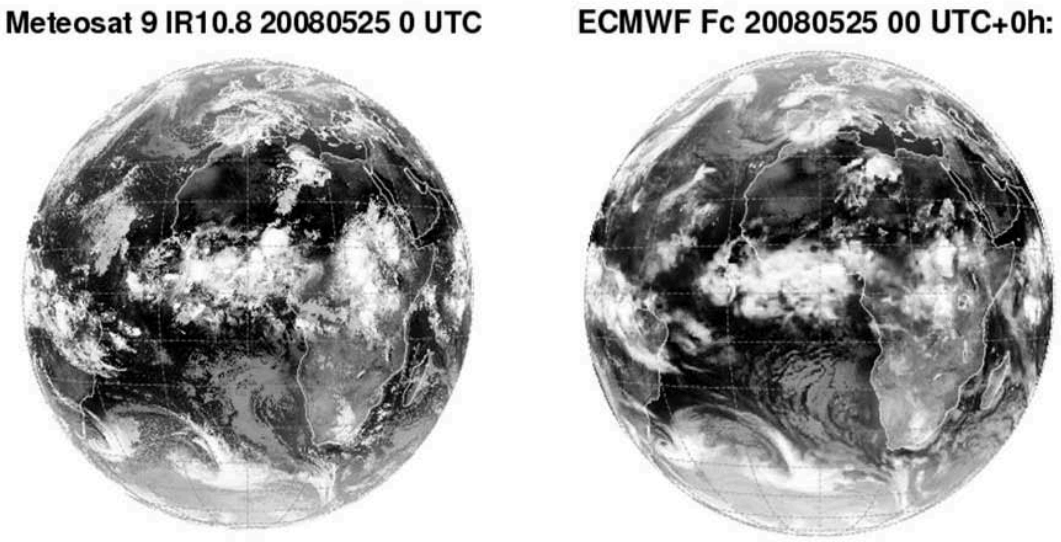

Figure 16: One frame from an animation of total cloud observations (OLR from METEOSAT) and forecast from a current ECMWF model.

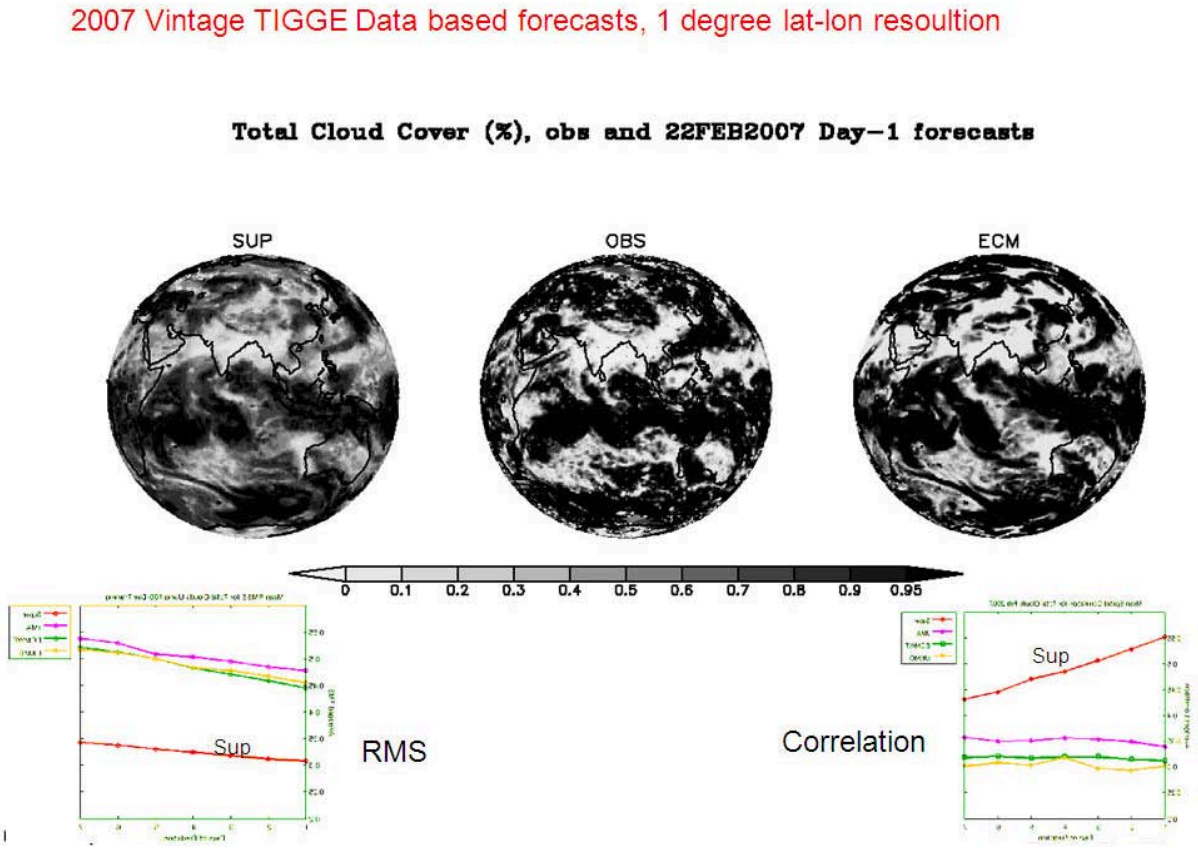

Figure 17: One frame from an animation of total cloud cover from the FSU Multimodel Superensemble, observations from ISCCP and forecast from a ECMWF model (2007 version), the film shows day 1 through 7 forecasts.

4.6. Superensemble based animation of total cloud forecasts for the 2007 vintage of models

At a composite TIGGE resolution of 1 degree latitude/longitude we show an animation of total clouds comparing the ISCCP based observed total clouds with the forecasts from the ECMWF (2007 Vintage interpolated to 1 degree resolution) and the FSU Superensemble based counterpart. One plot of that animation is shown in figure 17; here we see the three panels of the respective total clouds. Also shown at the bottom of this figure are the RMS errors and the spatial correlation skills for each day of forecast. Clearly the superensemble based forecasts at the TIGGE resolution from the 2007 vintage of models are superior to the skills of the member models. This animation through day 7 of forecasts suggests that models, for their total cloud forecasts, carry significant systematic errors, those can be reduced through the deployment of the multimodel superensemble.

5. Five day prediction of US rainfall at a 4 km resolution

FSU has developed a precipitation forecasting algorithm at very high resolution in space (4 Km) that holds much promise for North America. This utilizes a mix of radar and rain gauge data sets. This approach for high resolution precipitation forecasts rely on the use of a suite of multimodels. A downscaling component of our algorithm corrects the phase and amplitude errors of each member model forecast by using the special radar/raingauge data set at the 4 km resolution. This downscaling is being designed to translate the bias corrected member model forecasts down to the 4 km. The length span of forecasts covers through day ten for a domain covering the entire US (contiguous 48 States). The next step in this exercise is a training phase of a multimodel superensemble where the downscaled weights for the member model superensemble are obtained from the observed radar rain gauge observations of precipitation. The weights vary geographically at the resolution of 4km and also vary in time since different model's forecast errors are dependent on their respective forecast lengths. The last step in this exercise is to construct a downscaled multimodel superensemble, whose validation is again addressed against these same radar rain gauge rainfall products. Forecast assessment is carried out using various standard skill metrics such as RMS error, spatial correlations and the equitable threat scores and their bias scores. The US 4 km rainfall data sets: A best place to view this data is at a US National Weather Service web site: http://radar.weather.gov/Conus/full_loop.php

5.1. NCEP/EMC U.S. Gridded Radar-Estimated Precipitation

The National Centers for Environmental Prediction (NCEP) Environmental Modeling Center (EMC) produces a prototype, real-time, hourly, multi-sensor National Precipitation Analysis (NPA) in cooperation with the Office of Hydrology (OH). Approximately 3000 automated, hourly rain gauge observations are available over the contiguous 48 states via the GOES Data Collection Platform (DCP), and Automated Surface Observing Systems (ASOS). In addition, hourly digital precipitation (HD) radar estimates are obtained as compressed digital files via the Automation of Field Operations and Services (AFOS) network. (AFOS is now being replaced by Advanced Weather Interactive Processing System (AWIPS)). WSR-88D radar estimates are used to generate 131 x 131 (4 km) grid centered over each radar site. Bias correction of the radar estimates are performed using rain gauge data. A bias removed precipitation product is available since 2002 at every 6 hour (00Z, 06Z, 12Z, 18Z) interval; daily data is also available at 12Z. http://data.eol.ucar.edu/codiac/dss/id=21.092.

5.2. TIGGE Dataset

We use the TIGGE data sets of The Observing System Research and Predictability Experiment (THORPEX) program that are provided by NCAR see Table 1 below. Table 1 lists the prominent operational weather prediction models the from the TIGGE archive for the current period. The table identifies number of ensemble members, model resolution and forecast length. TIGGE datasets are the basis for the member model suite of the Florida State University superensemble. The multimodels included in our study are BOM (Australia), CMA (China), ECMWF (Europe), NCEP (USA) and UKMO (UK). TIGGE was designed at a workshop hosted in 2005 by the European Centre for Medium-Range Weather Forecasts (Richardson et al. 2005), with the ten centers officially joining between late 2006 and the present time. This archive is now available from the data archive centers at ECMWF, the China Meteorological Agency, and NCAR. Each day some 3108 files of 23 forecasts containing 469 GB (gigabytes) of data flow from the operational centers into the TIGGE system.

5.3. Statistical downscaling

Given the forecasts of precipitation from a number of forecast models with different horizontal resolutions (of the order of few 100 km), our downscaling for model precipitation follows three steps, Krishnamurti et al (2009). A simple bilinear interpolation of the model daily rain to the grid points of the observed rain (on 4 Km grid) is performed. This is done for each day of forecast for each model. Where ‘‘daily rain’’ refers to 24-h precipitation accumulation between 1200 and 1200 UTC the next day. While dealing with 6 hourly forecast same exercise can be repeated for 6 hourly forecasts. A time series of the interpolated rain is made for each model at every grid point and for each day of forecast separately (i.e., the string of day-1 forecasts). The same procedure is followed to generate strings for the day-2, -3, -4, and -5 forecasts. For each forecast lead time we have a string of high resolution, radar and rain gauge based rainfall observations. This provides an observational string. The downscaling strategy involves a linear regression of the time series of the data at each grid point:

$$Yi = a\,Xi + b$$

Where Xi are the rainfall forecasts (separately handled for each day and that had been subjected to bilinear interpolation), and Yi are the observed counterparts. The training period for our study is from 1 June 2007 to 31 August 2007. Based on 3-month training statistics, superensemble forecasts for the month of September are prepared. We utilize nearly 92 forecasts during the training phase of the superensemble to generate separate coefficients for the different member models. This is similar to our recent experience (Krishnamurti et al. 2006). These are calculated separately for each grid point of the IMD domain. The coefficients ‘*a*’ and ‘*b*’ thus vary from one grid location to the next and are also model dependent. The distribution of ‘*a*’ and ‘*b*’ provides useful information on the precipitation forecast bias of the member model. This exercise provides a bias corrected rainfall product for each of the member models for each day of forecast. If one downscales the model predicted precipitation alone, then the downscaled product would generally be an amplified version of the model’s precipitation. However, the superensemble that is next constructed using downscaled model forecasts takes it much further.

5.4. Superensemble methodology

The superensemble methodology is described in several past papers, Krishnamurti et al 2000a and 2000b. This will not be described here. All forecast validations for the downscaled superensemble are carried out using the 4 km observed radar/ raingauge rains.

5.5. Results on precipitation Forecasts at the 4km resolution:

In Fig 18 (a-c) the precipitation forecasts and the observed 4 km counterparts for days 1, 3 and 5 of forecasts are presented. These are 24 hour total rains from September 29 to September 30 2007 forecasted at different length. The four panels in these three illustrations show the precipitation forecasts (in mm/day) from the downscaled multimodel superensemble, ECMWF, JMA and the bottom right panel carries the radar /raingauge based observed estimates. This is one from a sample of 29 forecasts that were completed. Model rainfall validations utilize the 4 km observed rains directly for the downscaled superensemble. For the validation of TIGGE models we average the 4 km rains over grid squares of the TIGGE models prior to estimating skills such as the RMS errors and the pattern correlations. The RMS errors and the pattern correlations appear at the bottom left of each of the forecast panels; average rainfall for the domain is also shown in the right side of each panel. Basically these results show that at the 4 Km resolution the downscaled multimodel superensemble holds some promise, since it has the lowest RMS errors and the highest pattern correlations for the precipitation forecast through day 5 of forecasts. Two other examples of day 3 and 5 of forecasts are shown in figures 19 and 20, they carry similar information. This study derives mesoscale skills for the downscaled superensemble from downscaled large scale models during 90 days of past forecast during a training phase. Unlike mesoscale models that utilize grid sizes of the order of a few km, this is built entirely on TIGGE models as its starting point and appears to provide an alternate way for addressing mesoscale rainfall skills through day 5 of forecasts.

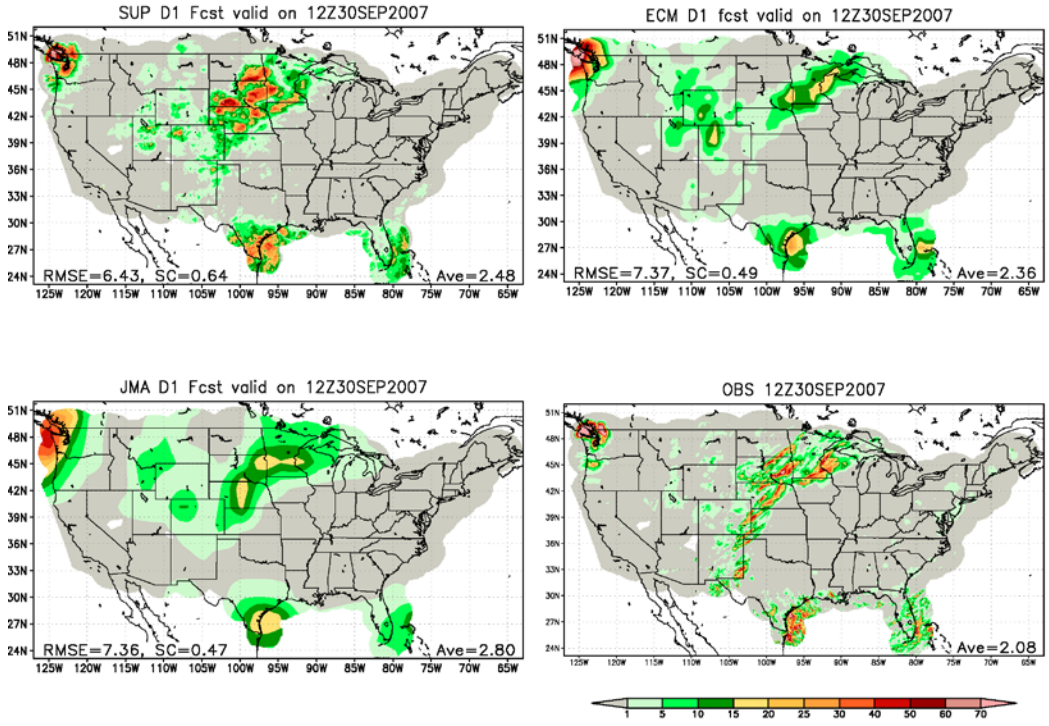

Figure 18 (a): Day one forecast of precipitation from the downscaled multimodel superensemble, ECMWF, JMA, and the observed radar raingauge product of US. These are 24 hour rainfall in unit's mm/day for 24 hour totals for days 0 to 1 day. The inset numbers in the bottom left denotes the RMS errors and pattern correlations of the forecast and the observed rains from the WSR radar and US dense rain gauge network, on the right side is the average value for the domain.

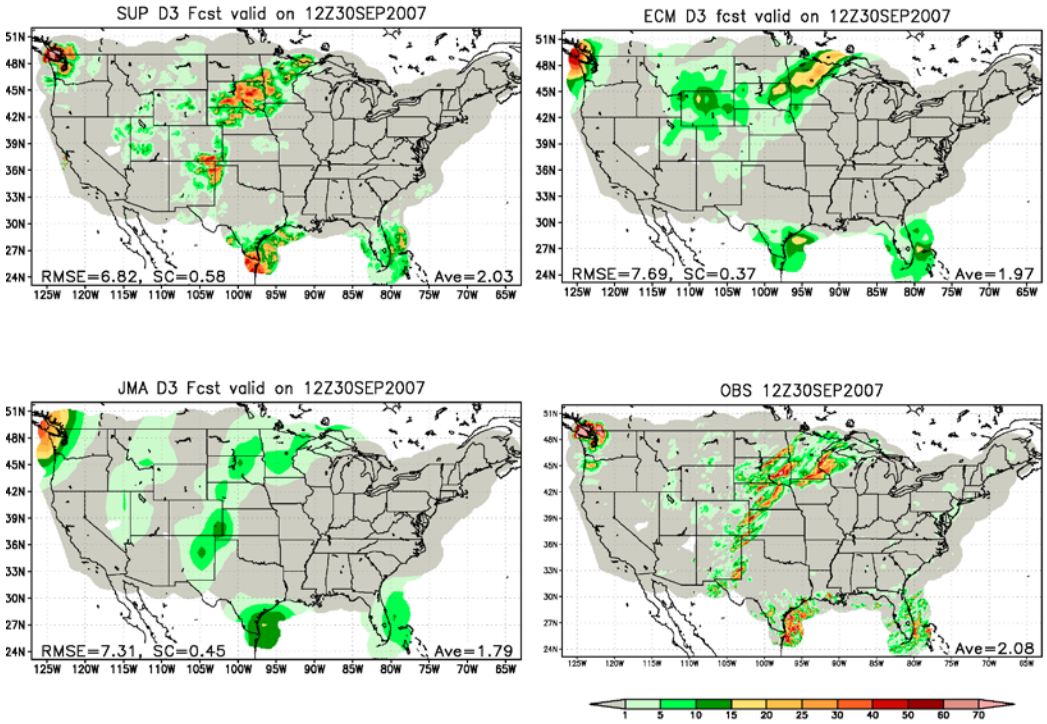

Figure 18 (b): *Same as Fig 18 (a) but for the day's 2 to 3 rainfall totals of forecasts and the observed rains.*

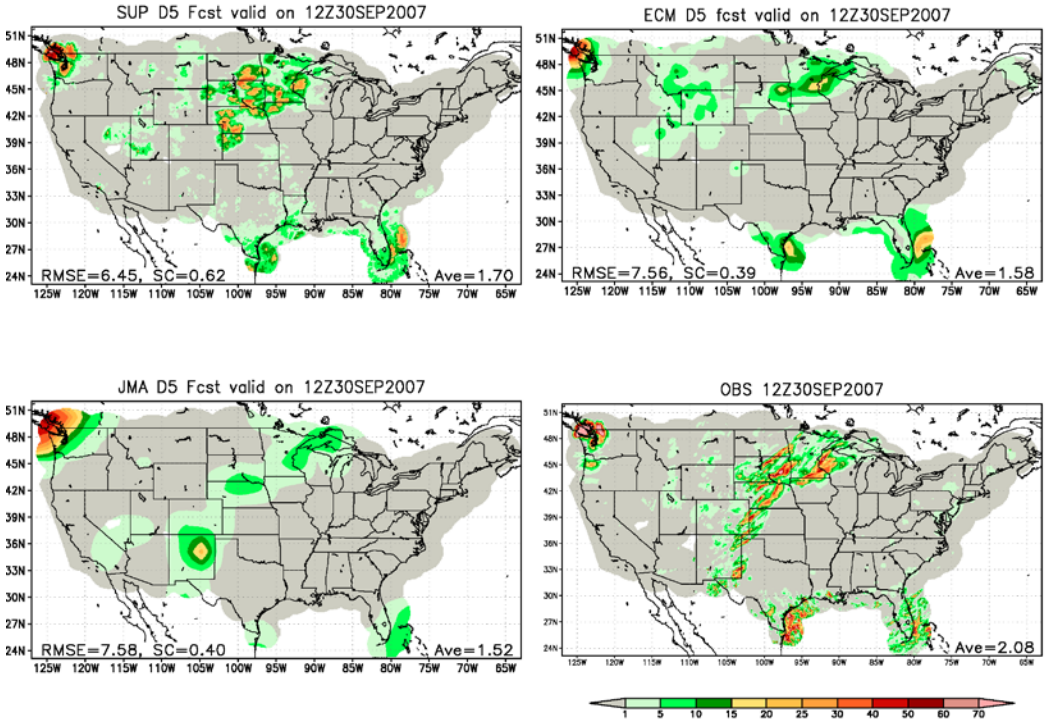

Figure 18 (c): *Same as Fig 18 (a) but for the day's 4 to 5 rainfall totals of forecasts and the observed rains.*

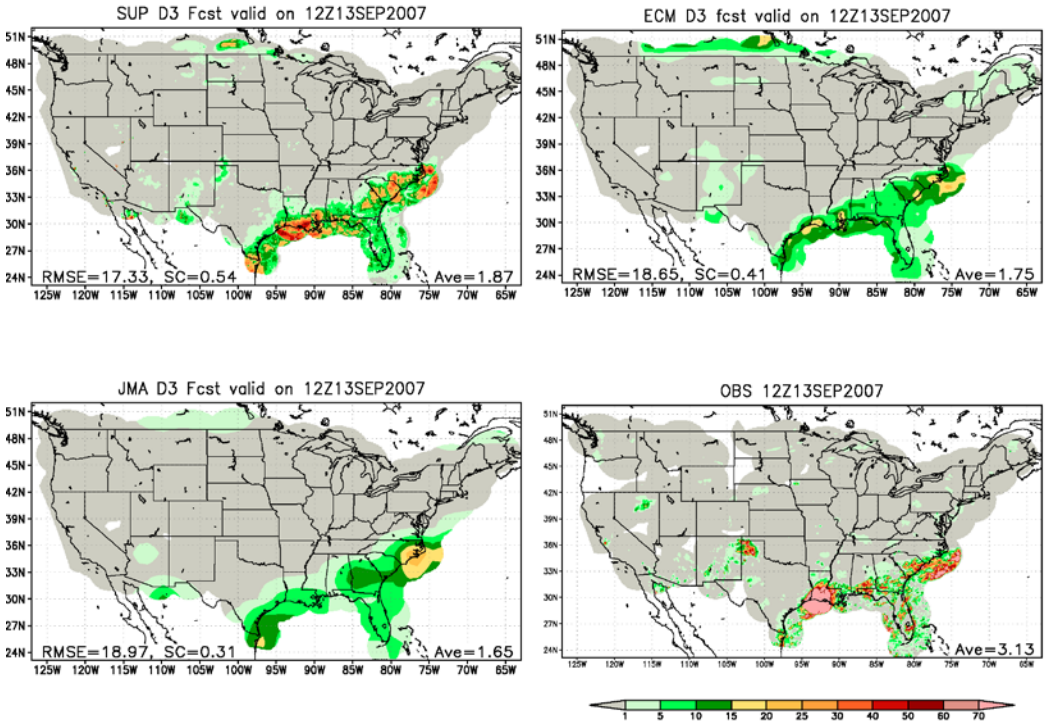

Figure 19: Another sample forecast for a day 3, valid on September 13th 2007, this follows the legend of Fig 18 (a).

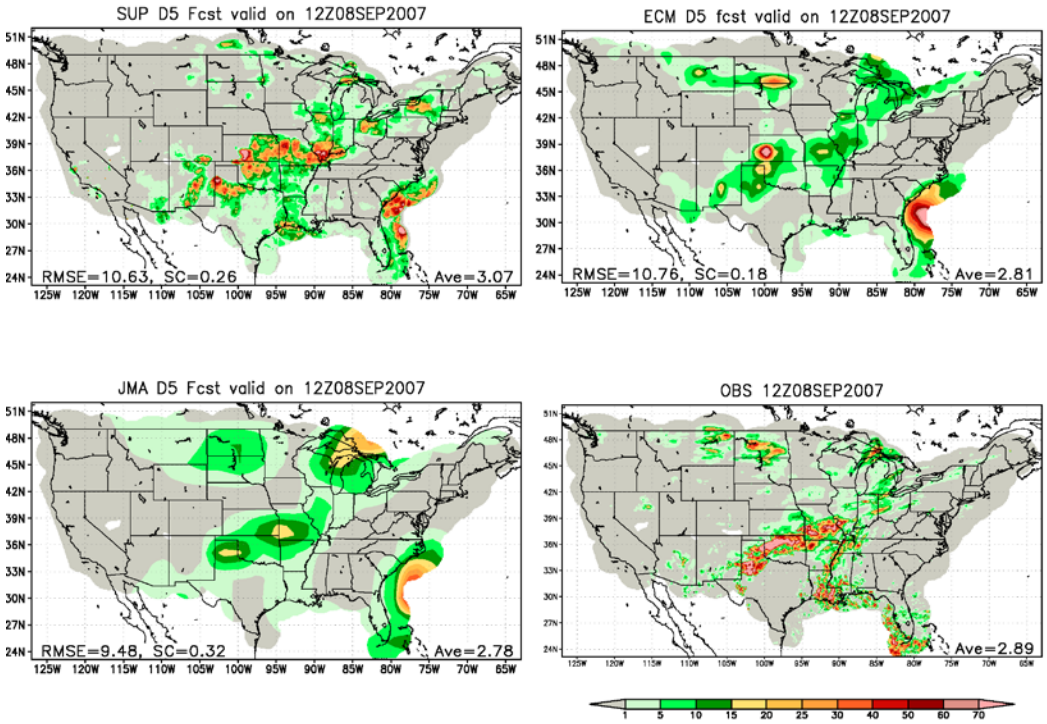

Figure 20: Another sample forecast for a day 5, valid on September 8th 2007, this follows the legend of Fig 18 (a).

Acknowledgements: We wish to acknowledge the financial support from NSF grant no.s ATM-0419618 and ATM-0533108 and NASA grant no. NNX09AC37G. Data support from CloudSat's DPC (Data Processing Center) team, ISCCP, MODIS, TIGGE and NCAR's Earth Observing Laboratory is greatly acknowledged.

References:

Bell, G.D., and D. Keyser, 1993: Shear and Curvature vorticity and Potential-Vorticity Interchanges: Interpretation and Application to a Cutoff Cyclone Event. *Mon. Wea. Rev.*, **121**, 76–102.

Chakraborty, A., T. N. Krishnamurti, 2006: Improved Seasonal Climate Forecasts of the South Asian Summer Monsoon Using a Suite of 13 Coupled Ocean-Atmosphere Models, *Monthly Weather Review*, **134,** 1697-1721

Davis, C., W. Wang, S.S. Chen, Y. Chen, K. Corbosiero, M. DeMaria, J. Dudhia, G. Holland, J. Klemp, J. Michalakes, H. Reeves, R. Rotunno, C. Snyder, and Q. Xiao, 2008: Prediction of Landfalling Hurricanes with the Advanced Hurricane WRF Model. Mon. Wea. Rev., 136, 1990–2005.

Geleyn, J.-F. 1981: Some diagnostics of the cloud-radiation interaction in the ECMWF forecasting model. Proc. Workshop on Radiation and Cloud-Radiation Interaction in Numerical Modelling, Reading, United Kingdom, ECMWF, 135–162.

Kalnay, E., M. Kanamitsu, R. Kistler, W. Collins, D. Deaven, L. Gandin, M. Iredell, S. Saha, G. White, J. Woollen, Y. Zhu, A. Leetmaa, R. Reynolds, M. Chelliah, W. Ebisuzaki, W. Higgins, J. Janowiak, K. Mo, C. Ropelewski, J. Wang, R. Jenne, and D. Joseph, 1996: The NCEP/NCAR 40-Year Reanalysis Project. *Bull. Amer. Meteor. Soc.*, **77**, 437–471.

Krishnamurti, T N, S. Pattnaik, L. Stefanova, T. S. V. Vijaya Kumar, B. P. Mackey, A. J. O'Shay and Richy Pasch. 2005b: The Hurricane Intensity Issue. *Monthly Wea Rev*: Vol. 133, No. 7, pp. 1886–1912

Krishnamurti, T. N., A. Chakraborty, A. Martin, W. K. Lau, K.-M. Kim, Y. Sud, and G. Walker., 2009: Impact of Arabian Sea pollution on the Bay of Bengal winter monsoon rains, *J. Geophys. Res.*, 114, D06213, doi:10.1029/2008JD010679.

Krishnamurti, T. N., A. Thomas, Anu Simon and Vinay Kumar. 2010: Desert air incursions, an overlooked aspect, for the dry spells of Indian summer monsoon, accepted for publication in *Journ. Of Atmosph. Sci.*

Krishnamurti, T. N., C. M. Kishtawal, Shin, D. W., C. E. Williford, 2000b: Improving tropical precipitation forecasts from a multi analysis superensemble. *J. Climate,* 13, 4217–4227.

Krishnamurti, T. N., P. Cunningham, and K. Rajendran, 2005a: Anomalous gradient winds in the subtropical jet stream and interpretations of forecast failures. *Meteor. Atmos. Phys.*,**88**, 237-250

Krishnamurti, T.N. & Lahouari Bounoua, 1996: *An Introduction to Numerical Weather Prediction Techniques.* CRC Press, Inc. USA.

Krishnamurti, T.N., A. Chakraborty, R. Krishnamurti, W.K. Dewar, and C.A. Clayson, 2006: Seasonal Prediction of Sea Surface Temperature Anomalies Using a Suite of 13 Coupled Atmosphere–Ocean Models. *J. Climate*, **19**, 6069–6088.

Krishnamurti, T.N., C.M. Kishtawal, T. LaRow, D. Bachiochi, Z. Zhang, C.E. Williford, S. Gadgil and S. Surendran, 1999: Improved skills for weather and seasonal climate forecasts from multi-model superensemble. *Science*, September 3, 1999.

Krishnamurti, T.N., C.M. Kishtawal, Z. Zhang, T. LaRow, D. Bachiochi, C.E. Williford, Gadgil, S. and S. Surendran, 2000a: Multi-model superensemble forecasts for weather and seasonal climate. *J. Climate*, **13**, 4196-4216.

LaRow, T. E. and T. N. Krishnamurti, 1998: Initial Conditions and ENSO Predictability using a Coupled Ocean Atmosphere Model. *Tellus*, 50A, 7694

Mogil, H. M., and R. L. Holle, 1972: Anomalous gradient winds: Existence and implications. *Mon. Wea. Rev.*,**100,** 709–715

Phillips, N. A. 1966. The equations of motion for a shallow rotating atmosphere and the "traditional approximation". *Mon. Weather Rev*., 23, 626-628

Rajeevan et al., 2006 Rajeevan, M., Bhate, J., Kale, J.D. and Lal, B, 2006: High resolution daily gridded rainfall data for the Indian region: Analysis of break and active monsoon spells. *Current Science*, **91**, 3, 296 – 306.

Richardson, D., R., Buizza and R. Hagedorn, 2005: Final report of the 1st Workshop on the THORPEX Interactive Grand Global Ensemble (TIGGE). WMO TD No. 1273, WWRP-THORPEX No. 5

Slingo, J. M., 1987: The development and verification of a cloud prediction scheme for the ECMWF model. Quart. J. R. Met. Soc., 113, 899-927.

Slingo, J.M., 1980: A cloud parameterization scheme derived from GATE data for use with a numerical model. Quart. J. R. Met. Soc., 106, 747-770.

Sundqvist, H., 1978: A parameterization scheme for non-convective condensation including prediction of cloud water content. Quart. J. R. Met. Soc., 104, 677-690.

Tiedtke, M ,. 1993: Representation of clouds in large-scale models. *Mon. Wea. Rev*, 121, 3040–3061

Viúdez,, and Haney (1996). Viúdez, A., and R.L. Haney, 1996: On the Shear and Curvature Vorticity Equations. *J. Atmos. Sci.*, **53**, 3384–3394.